January-March **2023** Volume **15** No.-**1** Pages: **1-42**

RMM
Revista de Osteoporosis y Metabolismo Mineral

Oficial Organ of Scientific Expression of the Sociedad Española de Investigación Ósea y del Metabolismo Mineral (SEIOMM)
and of the Sociedad Iberoamericana de Osteología y Metabolismo Mineral (SIBOMM)

www.revistadeosteoporosisymetabolismomineral.com

ARÁN Ediciones, S.L. ISSN (print version): 1889-836X. ISSN: (online version): 2173-2345

ROMM
Revista de Osteoporosis
y Metabolismo Mineral

Oficial Organ of Scientific Expression of the Sociedad Española de Investigación Ósea y del Metabolismo Mineral (SEIOMM)
and of the Sociedad Iberoamericana de Osteología y Metabolismo Mineral (SIBOMM)

Quarterly publication with 4 issues per year.

Indexes in which the journal is included:
Scielo, Web of Sciences, IBECS, Scopus, SIIC Data Bases, EMBASE, Redalyc, Emerging Sources Citation Index, Open J-Gate, DOAJ, Free Medical Journal, Google Academic, Medes, Electronic Journals Library AZB, e-revistas, WorldCat, Latindex, EBSCOhost, MedicLatina, Dialnet, SafetyLit, Mosby's, Encare, Academic Keys, ERIH plus, British Library, ROAD.

ISSN (print version): 1889-836X. ISSN: (online version): 2173-2345
Legal Deposit: M-8158-2023

ARÁN EDICIONES, S.L.

C/ Castelló, 128, 1.º - 28006 Madrid, Spain - Tel. 91 782 00 30 - Fax: 91 561 57 87
e-mail: osteoporosis@grupoaran.com
www.revistadeosteoporosisymetabolismomineral.com
www.grupoaran.com

ROMM
Revista de Osteoporosis y Metabolismo Mineral

Oficial Organ of Scientific Expression of the Sociedad Española de Investigación Ósea y del Metabolismo Mineral (SEIOMM) and of the Sociedad Iberoamericana de Osteología y Metabolismo Mineral (SIBOMM)

DIRECTORS

EDITORIAL COMMITTEE

seiomm Sociedad Española de Investigación Ósea y del Metabolismo Mineral
ARÁN

RMM
Revista de Osteoporosis
y Metabolismo Mineral

BOARD OF DIRECTORS OF THE SOCIEDAD ESPAÑOLA DE INVESTIGACIÓN ÓSEA Y DEL METABOLISMO MINERAL

ARÁN

RMM
Revista de Osteoporosis
y Metabolismo Mineral

Summary

Vol. **15** ■ January-March ■ **No.** 1

Cover image:
Plain X-ray of right knee in anteroposterior projection: large osteolytic lesion in the external distal region of the right femur. Hospital Universitario Marqué de Valdecilla. Santander

seiomm
Sociedad Española de Investigación Ósea y del Metabolismo Mineral

ARÁN

ARÁN

ROMM
Revista de Osteoporosis
y Metabolismo Mineral

The role of parathyroid hormone related protein (PTHrP) in bone metabolism: from basic to clinical research

INTRODUCTION

Interest in parathyroid hormone related protein (PTHrP) emerged from cancer-associated hypercalcemia, the most common paraneoplastic syndrome affecting up to 20 % of patients with advanced cancer (1). Back in the 1980s it was reported that most patients with tumor hypercalcemia showed characteristics of pseudo-hyperparathyroidism, which prompted thinking of PTH or a similar factor secreted by the tumor as the culprit of this syndrome. It was at the end of this decade when three independent groups isolated and characterized the true causal factor, which, as it turned out to be, showed a structural similarity with PTH in its N-terminal end; hence the name it is known for, PTHrP (2-4). PTHrP elevated plasma levels have been detected in most patients with tumor hypercalcemia (5,6) in whom PTHrP induces an increase of bone resorption and tubular calcium resorption as the cause of hypercalcemia.

However, its characterization led to an unexpected result: PTHrP turned out to be a cytokine that is present in a wide variety of normal tissues, where it exerts auto/paracrine and/or intracrine actions; as a matter of fact, tumor hypercalcemia is one of the few situations in which PTHrP exerts endocrine actions due to tumor hypersecretion (7). Therefore, the discovery of PTHrP is a magnificent example of translational research in biomedicine: the clinical research of a paraneoplastic syndrome ended up with the discovery of a new cellular cytokine. As a matter of fact, as we will see below, PTHrP "has come back to clinical research" somehow, as today it is regarded as a new agent in the pharmacological armamentarium of bone-forming agents in osteoporosis.

PTHrP: A MULTIFUNCTIONAL CYTOKINE IN BONE METABOLISM

The PTHrP gene contains multiple exons and is located in the short arm of chromosome 12, in a position analogous to that of the PTH gene in chromosome 11, and they both share a common ancestral origin. By alternative mRNA processing, the PTHrP gene in humans results in 3 protein isoforms of 139, 141, and 173 amino acids. Its proteolytic breakdown creates several fragments with different bioactivity (7,8) (Fig. 1). Its N-terminal fragment contains structural similarities with PTH, in both 1-13 and 14-34 regions, which allows its interaction with the same PTH receptor type 1 (PTHR1) (9). The middle region contains a nuclear/nucleolus localization domain (NLS) with specific functional properties in several cellular types including osteoblasts (10). The C-terminal fragment contains the (107-111) sequence (known as osteostatin), a powerful inhibitor of osteoclastic activity (11,12) whose osteogenic properties will be discussed below in this editorial.

PTHrP is abundant in bone tissue, being present in the bone marrow hematopoietic cells, chondrocytes, and osteoblastic lineage cells (8). The importance of the osseous role of PTHrP has been described in mice with genetic manipulation of its gene. The comparison of mice with homozygotic suppression of the PTHrP (-/-) or PTH (-/-) gene leads to interesting results: while the latter mice showed bone dimorphism but are viable, the former mice showed severe chondrodysplasia with reduced endochondral development and excessive mineralization causing death by asphyxiation of these unborn mice (13). PTH (-/-) mice in the post-natal stage show more trabecular bone associated with a PTHrP increase. As a matter of fact, this increase disappears when they are crossed with PTHrP (+/-) mice (14). Mice with PTHrP haploinsufficiency are viable and show early osteoporosis at 3 months of age, which is characterized in the appendicular skeleton by a reduction in bone volume and changes in trabecular structure, increased osteoblastic apoptosis, and osteoprogenitor deficit in the bone marrow (15). In addition, the anabolic effect of intermittently administered PTH (1-34) was more significant in these PTHrP (+/-) mice (15). This suggests that the different bony levels of PTHrP could explain the variability observed in the anabolic response to teriparatide [commercialized PTH (1-34)] in osteoporotic patients. These findings are indicative that PTHrP is an essential factor for trabecular bone maintenance during growth. Bone PTHrP deficiency could contribute to low bone formation in involutional osteoporosis since its expression is reduced in the long bones of old mice and in

primary human osteoblasts with the donor's age (16,17). In addition, mutant mice that express a truncated PTHrP (1-84) show delayed growth, as well as bone apoptosis, early senescence, and osteopenia (18). More recently by transfecting osteoblastic cells with plasmids that express mutated forms of PTHrP, we were able to prove an effect of the NLS domain on osteoblast viability and osteoblastic differentiation (10). In addition, the C-terminal region of PTHrP has proven capable of inhibiting IL-1beta-induced senescence in primary human osteoblast cultures from patients with arthrosis (19). *In vitro* studies have also demonstrated the capacity of the C-terminal fragment of PTHrP —similar to that of the N-terminal fragment homologous to PTH— to increase osteoblastic viability in primary human osteoblasts (20). Interestingly, this effect of the C-terminal PTHrP fragment turned out to be strictly dependent on the transactivation of vascular endothelial growth factor receptor-2 (VEGFR2) (20,21). The anti-apoptotic effect of PTHrP in osteoblasts is particularly important because it is an essential element in the PTH anabolic action (22).

Using the ovariectomized mouse as an established model of primary osteoporosis, our group was able to prove a similar efficacy of both PTHrP N- and C-terminal peptides administered every two days for 4 to 8 weeks to improve the deteriorated trabecular structure in the femur by using micro-computed tomography (μCT); an effect associated with an increase in osteocalcin, a bone formation marker, and an inhibition of resorptive markers, including the expression of the SOST gene in bone tissue and pyridinoline residues resulting from degradation of type 1 collagen in plasma (23). Andy F. Stewart et al. pioneered the use of PTHrP (1-36) to study its efficacy in humans with primary osteoporosis. The daily injection of this peptide at doses greater than that of PTH (40 μg) for 3 months in post-menopausal women caused a similar bone mineral density increase in the lumbar spine with both peptides, although it was greater in the hip (a predominantly cortical bone) and in the femoral neck with PTHrP. In addition, PTH increased the N-terminal propeptide and C-terminal telopeptides of type 1 collagen, bone formation and bone resorption markers, respectively, while PTHrP (1-36) only affected the first marker (24). More recently, a peptide derived from PTHrP (1-36) has been synthesized with 10 amino acidic substitutions in its C-terminal end —abaloparatide— which has proved effective increasing bone mass with lower risk of hypercalcemia compared to teriparatide treatment (25). Therefore, in a stage 2 clinical trial in post-menopausal women with severe osteoporosis it was observed that abaloparatide was more effective compared to teriparatide increasing bone mineral density in extravertebral skeletal locations. In addition, the double-blind, multicenter stage 3 placebo-controlled clinical trial Abaloparatide Comparator Trial In Vertebral Endpoints (ACTIVE) has demonstrated the greater efficacy of abaloparatide at 18 months reducing the risk of spinal and non-spinal fractures in this situation. Abaloparatide has been approved by the FDA for the management of post-menopausal osteoporosis with high risk of fractures. The differences of action on the resorptive component between PTH and PTHrP are attributed to their interaction with different PTHR1 conformations: PTH predominantly with G protein-independent conformation (R0) resulting in a prolonged AMPc response that favors the resorptive component through RANKL; PTHrP with a G protein-dependent conformation that induces a shorter response, thus favoring its anabolic action (25).

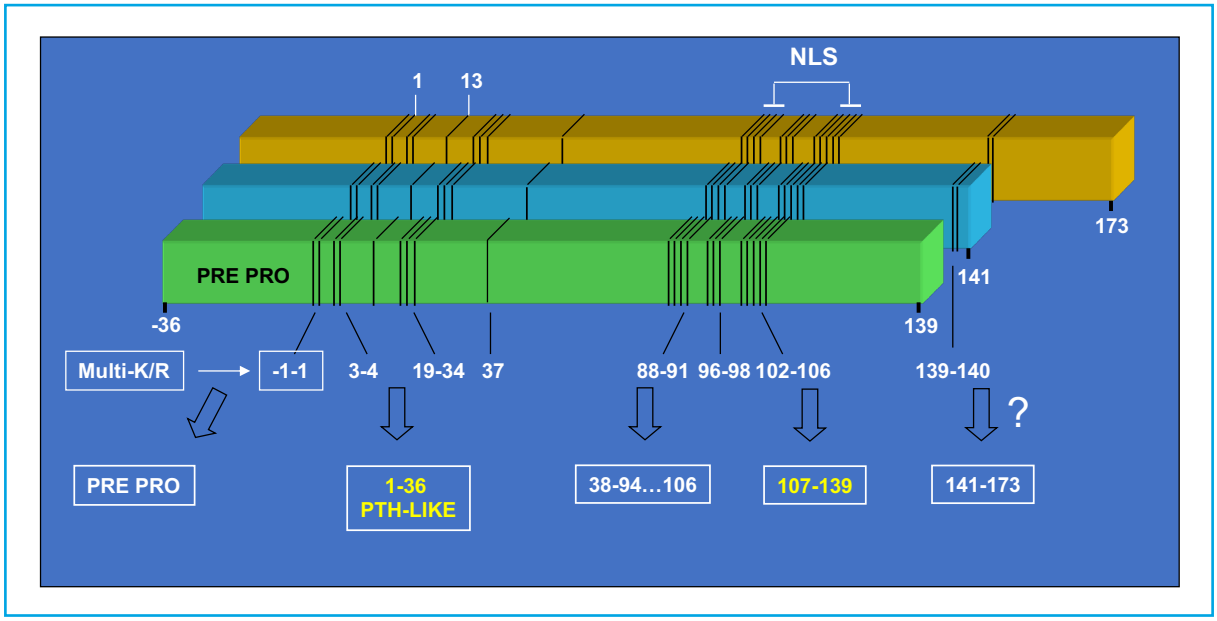

Figure 1. Processing of PTHrP protein isoforms.

Post-fracture bone regeneration can be compromised in osteoporosis and the current data indicate that systemic PTH is effective in this respect (26). Therefore, effectiveness of PTHrP was evaluated in an experimental bone regeneration model, medullary ablation in the tibia (27). Using osteoporotic mice treated with methylprednisolone, we demonstrated that the sequential administration (every 2 days) of PTHrP (1-36) or PTHrP (107-139) increased bone regeneration after medullary ablation (28). Taking this finding into account, we studied the possible osteo-regenerative effect of osteostatin, the sequence responsible for the anti-resorptive action of the C-terminal fragment of PTHrP (11), whose structural simplicity makes it especially attractive from a translational standpoint. Impregnation with osteostatin of mesoporous silica ceramics (SBA-15, synthesized and characterized by Prof. Vallet-Regí et al.) gives osteogenic properties to the biomaterial in murine osteoblast cultures of the MC3T3-E1 cell line (29). Implantation of this same material with osteostatin in a cavitary defect (that does not regenerate on its own) in the femoral epiphysis of healthy or osteoporotic rabbits induced new bone formation at 4-8 weeks in healthy animals (30), and at 2 weeks in osteoporotic rabbits (31). Subsequently, a biodegradable material (a gelatin-glutaraldehyde-coated hydroxyapatite polymer) was used impregnated with osteostatin or PTHrP (1-37) and implanted in a non-cavitary defect in the tibia of old osteopenic rats with or without diabetes *mellitus.* The presence of either PTHrP peptide in the graft induced the complete repair of the bone defect in a similar way at 4 weeks (32). An aspect particularly interesting in relation to osteostatin is that its *in vivo* anabolic action has been demonstrated in a diabetic mice model (with low bone formation). Dynamic bone histomorphometry demonstrated that treatment with equivalent doses of osteostatin or PTHrP (1-37) for 3 consecutive days normalized the decreased mineralize surface and the mineral apposition rate at 2 weeks, as well as bone formation, in the vertebrae of these mice (33).

In conclusion, PTHrP has turned out to be an essential factor for bone tissue development and maintenance. In addition, its osteogenic actions are not limited to its N-terminal region sharing structural similarities with PTH. The aspects discussed in this editorial have a special meaning considering the increased involutional osteoporosis associated with our longevity, which determines the growing demand for osteo-forming and osteo-regenerating molecules to repair fractures due to bone fragility. Therefore, basic and translational research have proven to be crucial to identify new PTHrP-based therapeutic strategies: in clinical use like abaloparatide or in potential development like osteostatin —a peptide derived from the C-terminal sequence of PTHrP— whose properties make it particularly attractive to promote bone formation and bone regeneration (Fig. 2).

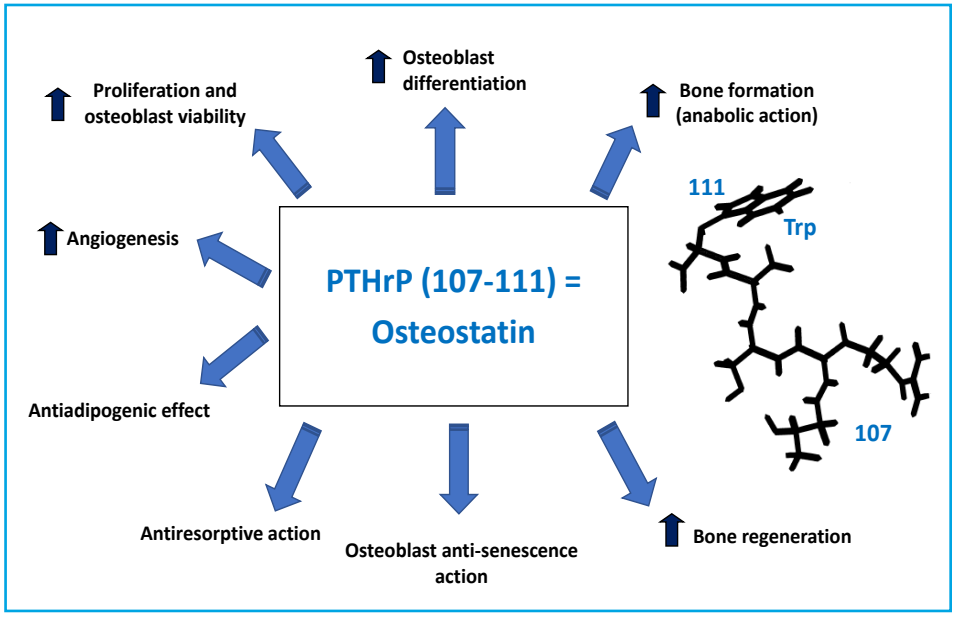

Figure 2. Osteogenic properties of osteostatin.

Conflict of interest: the author declares no conflict of interest.

Pedro Esbrit

Emeritus researcher. Instituto de Investigación Sanitaria-Fundación Jiménez Díaz. Madrid, Spain. Honorary Professor. Faculty of Pharmacy. Universidad Complutense de Madrid. Madrid, Spain

DOI: 10.20960/RevOsteoporosMetabMiner.00004

REFERENCES

1. Hurtado J, Esbrit P. Treatment of malignant hypercalcaemia. Expert Op Pharmacother 2002;3:521-7. DOI: 10.1517/14656566.3.5.521
2. Moseley JM, Kubota M, Diefenbach-Jagger H, Wettenhall RE, Kemp BE, Suva LJ, et al. Parathyroid hormone-related protein purified from a human lung cancer cell line. Proc Natl Acad Sci USA 1987;84:5048-52. DOI: 10.1073/pnas.84.14.5048
3. Burtis WJ, Wu T, Bunch C, Wysolmerski JJ, Insogna KL, Weir EC, et al. Identification of a novel 17,000-dalton parathyroid hormone-like adenylate cyclase-stimulating protein from a tumor associated with humoral hypercalcemia of malignancy. J Biol Chem 1987;262:7151-6.
4. Strewler GJ, Stern PH, Jacobs JW, Eveloff J, Klein RF, Leung SC, et al. Parathyroid hormone-like protein from human renal carcinoma cells: structural and functional homology with parathyroid hormone. J Clin Invest 1987;80:1803-7. DOI: 10.1172/JCI113275
5. De Miguel F, Motellón JL, Hurtado J, Jiménez FJ, Esbrit P. Comparison of two immunoradiometric assays for parathyroid hormone-related protein in the evaluation of cancer patients with and without hipercalcemia. Clin Chim Acta 1998;277:171-80. DOI: 10.1016/s0009-8981(98)00127-2
6. Motellón JL, Jiménez FJ, de Miguel F, Jaras MJ, Díaz A, Hurtado J, et al. Parathyroid hormone-related protein, parathyroid hormone, and vitamin D in hypercalcemia of malignancy. Clin Chim Acta 2000;290:189-97. DOI: 10.1016/s0009-8981(99)00181-3
7. Martin TJ, Mosely JM, Williams ED. Parathyroid hormone-related protein: hormone and cytokine. J Endocrinol 1997;154:S23-37.
8. Philbrick WM, Wysolmerski JJ, Galbraith S, Holt E, Orloff JJ, Yang KH, et al. Defining the roles of parathyroid hormone-related protein in normal physiology. Physiol Rev 1996;76:127-73. DOI: 10.1152/physrev.1996.76.1.127
9. Gardella TJ, Vilardaga JP. International union of basic and clinical pharmacology. XCIII. The parathyroid hormone receptors — Family B G protein-coupled receptors. Pharmacol Rev 2015;67:310-37. DOI: 10.1124/pr.114.009464
10. García-Martín A, Ardura JA, Maycas M, Lozano D, López-Herradón A, Portal-Núñez S, et al. Functional roles of the nuclear localization signal of parathyroid hormone-related protein (PTHrP) in osteoblastic cells. Mol Endocrinol 2014;28:925-34. DOI: 10.1210/me.2013-1225
11. Fenton AJ, Kemp BE, Hammonds RG, Jr., Mitchelhill K, Moseley JM, Martin TJ, et al. A potent inhibitor of osteoclastic bone resorption within a highly conserved pentapeptide region of parathyroid hormone-related protein; PTHrP [107–111] Endocrinology 1991;129:3424-6. DOI: 10.1210/endo-129-6-3424
12. Ibáñez L, Nácher-Juan J, Terencio MC, Ferrándiz ML, Alcaraz MJ. Osteostatin inhibits M-CSF+RANKL-induced human osteoclast differentiation by modulating NFATc1. Int J Mol Sci 2022;23:8551. DOI: 10.3390/ijms23158551
13. Karaplis AC, Luz A, Glowacki J, Bronson RT, Tybulewicz VLJ, Kronenberg HM, et al. Lethal skeletal dysplasia from targeted disruption of the parathyroid hormone-related peptide gene. Genes Devel 1994;8:277-89. DOI: 10.1101/gad.8.3.277
14. Miao D, Jiarong L, Yingben X, Su H, Karaplis AC, Goltzman D. Parathyroid hormone-related peptide is required for increased trabecular bone volume in parathyroid hormone-null mice. Endocrinology 2004;145:3554-62. DOI: 10.1210/en.2003-1695
15. Miao D, He B, Jiang Y, Kobayashi T, Sorocéanu MA, Zhao J, et al. Osteoblast-derived PTHrP is a potent endogenous bone anabolic agent that modifies the therapeutic efficacy of administered PTH 1-34. J Clin Invest 2005;115:2402-11. DOI: 10.1172/JCI24918
16. Portal-Núñez S, Manassra R, Lozano D, Acitores A, Mulero F, Villanueva-Peñacarrillo ML, et al. Characterization of skeletal alterations in a model of prematurely aging mice. Age (Dordr) 2013;35:383-93. DOI: 10.1007/s11357-011-9372-8
17. Martínez P, Esbrit P, Rodrigo A, Alvarez-Arroyo MV, Martínez ME. Age-related changes in parathyroid hormone-related protein and vascular endothelial growth factor in human osteoblastic cells. Osteoporosis Int 2002;13:874-81. DOI: 10.1007/s001980200120
18. Miao D, Su H, He B, Gao J, Xia Q, Zhu M, et al. Severe growth retardation and early lethality in mice lacking the nuclear localization sequence and C-terminus of PTH-related protein. Proc Natl Acad Sci U S A 2008;105:20309-14. DOI: 10.1073/pnas.0805690105
19. Platas J, Guillén MI, Gomar F, Castejón MA, Esbrit P, Alcaraz MJ. Anti-senescence and anti-inflammatory effects of the C-terminal moiety of PTHrP peptides in OA osteoblasts. J Gerontol A Biol Sci Med Sci 2017;72:624-31. DOI: 10.1093/gerona/glw100
20. Alonso V, de Gortázar AR, Ardura JA, Andrade-Zapata I, Alvarez-Arroyo MV, Esbrit P. Parathyroid hormone-related protein (107-139) increases human osteoblastic cell survival by activation of vascular endothelial growth factor receptor-2. J Cell Physiol 2008;217:717-27. DOI: 10.1002/jcp.21547
21. Esbrit P, Alcaraz MJ. Current perspectives on parathyroid hormone (PTH) and PTH-related protein (PTHrP) as bone anabolic therapies. Biochem Pharmacol 2013;85:1417-23. DOI: 10.1016/j.bcp.2013.03.002
22. Jilka RL, Weinstein RS, Bellido T, Roberson P, Parfitt AM, Manolagas SC. Increased bone formation by prevention of osteoblast apoptosis with parathyroid hormone. J Clin Invest 1999;104:439-46. DOI: 10.1172/JCI6610
23. De Castro LF, Lozano D, Portal-Núñez S, Maycas M, de la Fuente M, Caeiro JR, et al. Comparison of the skeletal effects induced by daily administration of PTHrP (1-36) and PTHrP (107-139) to ovariectomized mice. J Cell Physiol 2012;227:1752-60. DOI: 10.1002/jcp.22902
24. Horwitz MJ, Augustine M, Kahn L, Martin E, Oakley CC, Carneiro RM, et al. A comparison of parathyroid hormone-related protein (1-36) and parathyroid hormone (1-34) on markers of bone turnover and bone density in postmenopausal women: the PrOP study. J Bone Miner Res 2013;28:2266-76. DOI: 10.1002/jbmr.1978
25. Ardura JA, Portal-Núñez S, Alonso V, Bravo B, Gortázar AR. Handling parathormone receptor type 1 in skeletal diseases: realities and expectations of abaloparatide. Trends Endocrinol Metab 2019;30:756-66. DOI: 10.1016/j.tem.2019.07.014
26. Hong H, Song T, Liu Y, Li J , Jiang Q, Song Q, et al. The effectiveness and safety of parathyroid hormone in fracture healing: A meta-analysis. Clinics (Sao Paulo) 2019;74:e800. DOI: 10.6061/clinics/2019/e800
27. Ono N, Nakashima K, Schipani E, Hayata T, Ezura Y, Soma K, et al. Constitutively active PTH/PTHrP receptor specifically expressed in osteoblasts enhances bone formation induced by bone marrow ablation. J Cell Physiol 2012;227:408-15. DOI: 10.1002/jcp.22986

28. De Castro LF, Lozano D, Dapía S, Portal-Núñez S, Caeiro JR, Gómez-Barrena E, et al. Role of the N- and C-terminal fragments of parathyroid hormone-related protein as putative therapies to improve bone regeneration under high glucocorticoid treatment. Tissue Eng Part A 2010;16:1157-68. DOI: 10.1089/ten.TEA.2009.0355
29. Lozano D, Manzano M, Doadrio JC, Salinas AJ, Vallet-Regí M, Gómez-Barrena E, et al. Osteostatin-loaded bioceramics stimulate osteoblastic growth and differentiation. Acta Biomater 2010;6:797-803. DOI: 10.1016/j.actbio.2009.08.033
30. Trejo CG, Lozano D, Manzano M, Doadrio JC, Salinas AJ, Dapía S, et al. The osteoinductive properties of mesoporous silicate coated with osteostatin in a rabbit femur cavity defect model. Biomaterials 2010;31:8564-73. DOI: 10.1016/j.biomaterials.2010.07.103
31. Lozano D, Trejo CG, Gómez-Barrena E, Manzano M, Doadrio JC, Salinas AJ, et al. Osteostatin-loaded onto mesoporous ceramics improves the early phase of bone regeneration in a rabbit osteopenia model. Acta Biomater 2012;8:2317-23. DOI: 10.1016/j.actbio.2012.03.014
32. Ardura JA, Portal-Núñez S, Lozano D, Gutiérrez-Rojas I, Sánchez-Salcedo S, López-Herradón A, et al. Local delivery of parathyroid hormone-related protein-derived peptides coated onto a hydroxyapatite-based implant enhances bone regeneration in old and diabetic rats. J Biomed Mater Res A 2016;104:2060-70. DOI: 10.1002/jbm.a.35742
33. Maycas M, McAndrews KA, Sato AY, Pellegrini GG, Brown DM, Allen MR , et al. PTHrP-derived peptides restore bone mass and strength in diabetic mice: Additive effect of mechanical loading. J Bone Miner Res 2017;32:486-97. DOI: 10.1002/jbmr.3007

ROMM
Revista de Osteoporosis y Metabolismo Mineral

Original

Osteoclast generation from RAW 264.7 and PBMC cells. The set up in our lab

Susana Jurado[1,2], Albert Parés[1,3], Pilar Peris[2], Andrés Combalia[4], Ana Monegal[2], Nuria Guañabens[1,2]

[1]Center of Biomedical Research in Liver and Digestive Diseases (CIBERehd). Spain. [2]Metabolic Bone Diseases Unit. Department of Rheumatology; [3]Liver Unit; and [4]Traumatology Unit. Hospital Clínic de Barcelona. IDIBAPS Universitat de Barcelona. Barcelona, Spain

Abstract

Introduction and objectives: osteoclasts are terminally differentiated giant multinucleated cells derived from the fusion of mononuclear progenitors of the monocyte/macrophage hematopoietic lineage. The objective of our group was to achieve the best method for osteoclast differentiation, from both RAW 264.7 cells and peripheral blood monocytes.

Material and methods: RAW 264.7 cells and human PBMCs were differentiated into osteoclasts. Success in differentiation was assessed by TRAP staining. Osteoclast activity was detected by the resorption pits in Corning® Osteo Assay Surface Plates.

Results: the optimal cell density for RAW 264.7 cell differentiation was 25,000 cells/cm^2 with 30 ng/mL of RANKL for 6 days. Osteoclasts differentiated from PBMCs were observed after 4 weeks with 25 ng/mL M-CSF and 30 ng/mL RANKL. Individual pits or multiple pit clusters were observed on the surface plates.

Conclusions: we report optimal conditions for the differentiation of osteoclasts from

Keywords:
Osteoclasts.
Differentiation.
Bone resorption.

Received: 26/05/2022 • Accepted: 25/09/2022

Conflict of interest: the authors declare no conflict of interest.

Jurado S, Parés A, Peris P, Combalia A, Monegal A, Guañabens N. Osteoclast generation from RAW 264.7 and PBMC cells. The set up in our lab. Rev Osteoporos Metab Miner 2023;15(1):6-11

DOI: 10.20960/RevOsteoporosMetabMiner.00005

Correspondence:
Susana Jurado. Metabolic Bone Diseases Unit. Department of Rheumatology. Hospital Clínic de Barcelona. C/ Villarroel, 170. 08036 Barcelona, Spain
e-mail: susanajurado80@gmail.com

INTRODUCTION

The bone is a dynamic tissue which is under constant remodeling. Indeed, bone remodeling is a complex cellular process that involves bone resorption induced by osteoclasts and bone formation produced by osteoblasts (1). An imbalance in this equilibrium results in metabolic bone diseases such as osteoporosis or osteopetrosis. This disequilibrium may be produced by an increase in bone resorption due to a rise in the number of osteoclasts or in their activity, or by a decrease in bone formation due to a lower osteoblast activity, or by both combined effects.

The direct cellular interactions between osteoblasts and osteoclasts, mediated in part by the receptor activator of NF-κB, its ligand and osteoprotegerin (RANK/RANKL/OPG) pathway, are essential for the regulation of bone remodeling (2). The interaction between RANKL, either at the osteoblast surface or in its soluble form and its receptor RANK, on the membrane of osteoclast precursors initiates a cascade of signaling events, resulting in their differentiation to form mature osteoclasts. OPG, an osteoblast-secreted glycoprotein of the tumor necrosis factor receptor superfamily, acts as a decoy receptor and blocks the interaction between RANKL and RANK. Moreover, many other cytokines and hormones have been found to regulate either OPG or RANKL, or both, in similar or opposite directions (3).

Osteoclasts represent 1-2 % of the total bone resident cells. They are terminally differentiated giant multinucleated cells, derived from the fusion of mononuclear progenitors of the monocyte/macrophage hematopoietic lineage (1). The importance of osteoclasts in bone homeostasis is evidenced by the diseases in which osteoclast formation or function is unbalanced. However, the role of osteoclasts in health or disease and its biology have remained elusive for years. Initially, it was thought that osteoclasts were cells that undergo apoptosis after a short lifespan of around two weeks, but in the last few years, it has been shown that osteoclasts have a lifespan of around 6 months. A recent study has revealed that mature osteoclasts are capable of fissioning into smaller daughter cells, a new cell type called osteomorphs (4). These osteomorphs are freely motile cells, able to migrate and fuse with other osteomorphs or osteoclasts, creating recycled cells (4).

Osteoclasts can be studied *in vitro* by isolating primary bone marrow or peripheral blood monocytes cells (PBMCs), or by using the murine myeloid cell line RAW 264.7, which can be differentiated into mature osteoclasts (5-7). The use of established cell lines like RAW 264.7 instead of human primary cell cultures is extensive because it is not feasible to cultivate and expand osteoclasts for long periods of time. In addition, available cell numbers from single differentiation experiments are limited and experimental outcome may be variable depending on the cell donor. Therefore, the use of the RAW 264.7 cell line, which is quite extended, avoids these problems.

In the literature, the differentiation process of osteoclasts from RAW 264.7 cells is well established. However, the differentiation process of osteoclasts from human PBMCs is not clearly described. Thus, in scientific reports there is no defined cell density or time required to achieve the desired osteoclasts. We needed much bibliographic research in the first place, and then we performed different technical approaches to obtain osteoclasts until suitable differentiation results were achieved. All of these tasks required up to a month for the process to be completed.

Therefore, the aim of this study was to optimize osteoclast differentiation techniques, from both RAW 264.7 cells and peripheral blood monocytes. The goal was to obtain differentiated osteoclasts in order to perform experiments with substances that act on the viability and apoptosis of osteoclasts.

MATERIAL AND METHODS

MATERIALS

Alpha-minimum essential medium (aMEM), Dulbecco's modified Eagle medium (DMEM), fetal bovine serum (FBS), Phosphate Buffered Saline (PBS), l-glutamine and trypsin were purchased from Invitrogen (Thermo Fisher Scientific) (Waltham, MA, USA); accutase and toluidine blue were purchased from Sigma Chemical Co. (St. Louis, MO, USA); penicillin-streptomycin from LabClinics (Barcelona, Spain); recombinant mouse RANKL, recombinant human RANKL and recombinant human M-CSF from R&D systems (Bio-Techne, UK); RosetteSep™ Human Monocyte Enrichment Cocktail and Lymphoprep™ were purchased from Stemcell Technologies (Köln, Germany).

OSTEOCLASTS FROM RAW 264.7 CELL CULTURE

RAW 264.7 cells, a transformed murine monocytic macrophage cell line from the European Collection of Authenticated Cell Cultures (ECACC, England), were cultured at 37 °C in 5 % CO_2 atmosphere in DMEM, supplemented with 10 % heat-inactivated FBS and 100 U/mL penicillin-streptomycin. Cells were plated directly on 96-well plates at a density of 1.5 x 10^4, 2.5 x 10^4 and 3.5 x 10^4 cells/cm^2. The medium used for osteoclastic differentiation was aMEM supplemented with 10% heat-inactivated FBS, 100 U/mL penicillin-streptomycin and 25, 30 and 50 ng/mL of recombi-

nant mouse RANKL. The medium was removed and replaced with fresh medium every 48 h-72 h. After 6 days, RAW 264.7 cells were differentiated into osteoclasts.

OSTEOCLASTS FROM PERIPHERAL BLOOD MONOCYTE CULTURE

RosetteSep™ Human Monocyte Enrichment Cocktail™ was used to purify human monocytes taken from total PBMCs of buffy coats, supplied by the local reference blood bank (Banc de Sang i Teixits, Barcelona). Cells were separated using Lymphoprep™, following the manufacturer's protocol.

Cells were seeded in two different ways. For the first attempt, they were seeded in a 75 cm^2 flask at a density of 150,000 cells/cm^2, and then cultured at 37 °C in 5 % CO_2 atmosphere in aMEM, supplemented with 10 % heat-inactivated FBS, 100 U/mL penicillin-streptomycin and 25 ng/mL of recombinant human macrophage colony-stimulating factor (M-CSF) for 2 weeks. The medium was replaced every 48 to 72 hours. Then, cells were treated with accutase and plated on 96-well plates at a density of 80,000 cells/cm^2 for one additional week, adding 30 ng/mL of recombinant human RANKL to the medium. Human monocytes were differentiated into osteoclasts. On the other hand, cells were seeded directly on 96-well plates at a density of 150,000, 250,000 and 400,000 cells/cm^2 and were treated from the beginning with both 25 ng/mL of recombinant human M-CSF and 30 ng/mL of recombinant human RANKL in aMEM supplemented with 10 % heat-inactivated FBS, 100 U/mL penicillin-streptomycin for three-four weeks.

CHARACTERIZATION OF OSTEOCLASTS AND RESORPTION PIT FORMATION ASSAY

To identify the generation of multinucleated osteoclasts, cells were stained for the enzyme tartrate-resistant acid phosphatase (TRAP) using the TRAP-staining kit (Sigma-Aldrich, St. Louis, MO, USA), according to the manufacturer's instructions. TRAP-positive multinucleated (3 or more nuclei) cells were visualized by light microscopy. Each osteoclast characterization assay was performed at least 3 times.

Resorption pits were assessed by seeding RAW 264.7 cells to differentiate into osteoclasts at a density of 25,000 cells/cm^2 on 24-well Corning® Osteo Assay Surface Plates (Corning Cat. No. 3987, Cultek, Life Sciences, NY, USA). Cells were then removed and well surfaces were stained with 1 % toluidine blue for 1 min. Individual resorption pits or multiple pit clusters were visualized on the surfaces by light microscopy.

Images were obtained using a DM IL LED-inverted microscope with a MC190 HD camera and the Application Suit v3.4.0 acquisition software (Leica microsistemas SLU, Spain). The area of pits was analyzed using Image J software (NIH, Bethesda, MD, USA).

RESULTS

DIFFERENTIATION AND IDENTIFICATION OF OSTEOCLASTS

The optimal cell density for RAW 264.7 differentiation cells was 25,000 cells/cm^2. A concentration of 30 ng/mL of RANKL was enough to achieve an optimal differentiation. Under this condition, multinucleated osteoclasts were observed by TRAP staining after 5-7 days (Fig. 1). Osteoclastic ruffled border and connections between multinucleated osteoclasts were observed as well (Fig. 1). However, we obtained no differentiated osteoclasts when monocytes were plated directly on 96-well plates, being the method by which we differentiated RAW into osteoclasts. By contrast, in the case of monocytes from PBMCs, the cells remained monocyte-like after 3-4 weeks on 96-well plates and differences in the doses of RANKL and M-CSF did not change this result. We did not differentiate the cells by putting glass coverslips on the wells, as recommended by some research groups, since from our perspective, this technical approach did not bring advantages and made the methodology more complex. For this reason, we opted to maintain the cells in 75 cm^2 flasks for the time being by administering only M-CSF to keep the cells in a resting and stable state. After 3 weeks, we finally transferred the cells to 96-well plates and started administering RANKL as well. In this manner, we were able to observe differentiated osteoclasts within another week. In the differentiation process into osteoclasts from PBMCs, multinucleated osteoclasts were observed by TRAP staining after 3-4 weeks, as shown in figure 2.

RESORPTION PITS

Individual pits or multiple pit clusters were observed using a microscope at 10x magnifications in the Corning® Osteo Assay surface plates (Fig. 3). When activators of osteoclast activity such as bilirubin were added, more resorbed areas were observed compared to the non-treated plates (data not shown). Indeed, we found that bilirubin was an activator of osteoclast survival in our viability studies, resulting in an increase in osteoclast number and activity, identified by observing the resorption pits on the Corning® Osteo Assay surface plates.

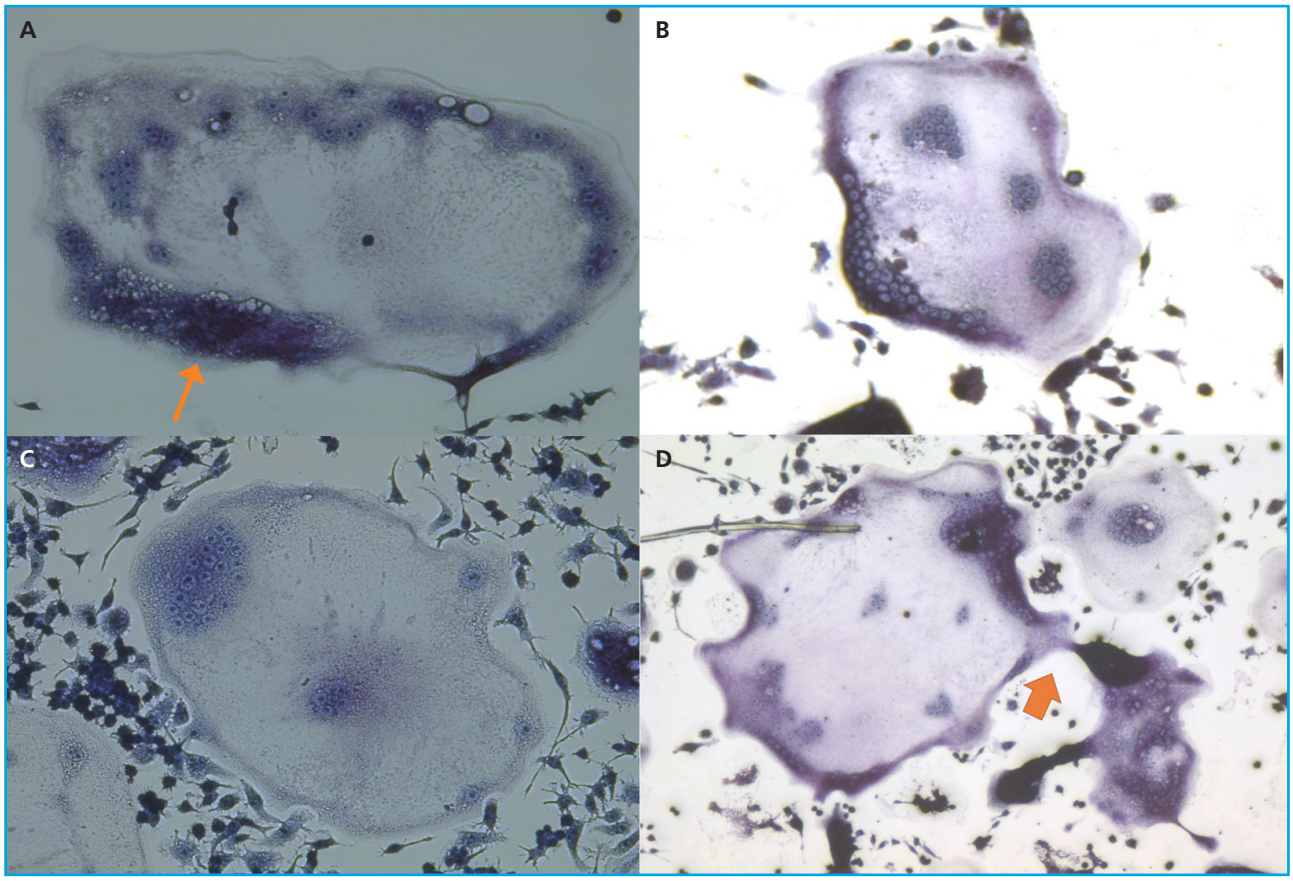

Figure 1. Differentiated osteoclasts from RAW 264.7 cells are shown after TRAP staining. Big multinucleated osteoclasts are shown. Ruffled border (1A, thin arrow) and connections between multinucleated osteoclasts (1D, thick arrow) are observed. Experiments were performed more than 10 times.

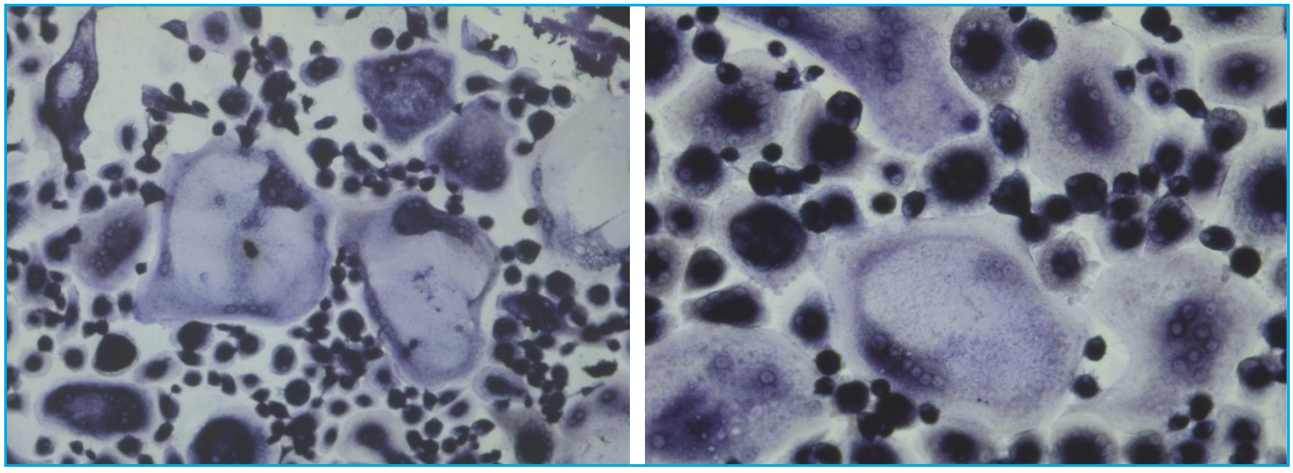

Figure 2. Differentiated osteoclasts from human PBMCs after TRAP staining are represented. Many multinucleated osteoclasts were observed. Experiments were performed more than 10 times.

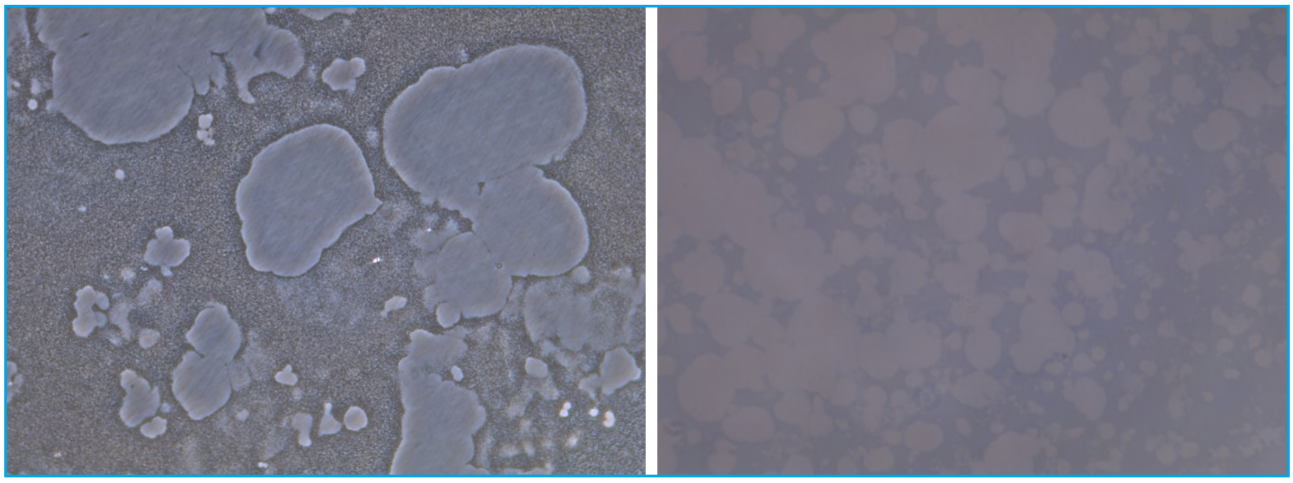

Figure 3. Representative images of the pit resorption areas on Corning® Osteo Assay Surface Plates are shown (clear areas). Differentiated osteoclasts from RAW 264.7 cells were plated. Experiment was performed once.

DISCUSSION

Osteoclasts are fascinating cells for their abilities and functions. Their tight balance with osteoblasts is regulated by multiple factors that make a very accurate process. With the recent discovery of osteomorphs by McDonald et al. (4), this process has turned out to be even more precise. Osteomorphs will remain waiting until the moment in which mature osteoclasts are required to resorb bone.

In our experience, the differentiation process of the cells is not free of technical difficulties. Several factors could act on this process, and osteoclasts may not become active, or simply not correctly differentiated. The differentiation of osteoclasts from RAW 264.7 cells was easier than with primary human cells, because it was a simpler process with more cell availability, and in addition, the time to achieve differentiated cells was shorter than with primary cells. We found several bibliographic references as a guide to begin with and we found our optimal concentrations of both RANKL and RAW 264.7 cells in a short time. However, the differentiation of osteoclasts from monocytes of human PBMCs was complex. First, the heterogeneity that we found in the literature was high, and it was difficult to decide how to start our experiments. Secondly, monocytes take a long time to become osteoclasts. Moreover, the diffentiation process was more expensive than using RAW cells because in this case, two differentiating activators were needed: the human M-CSF and RANKL. Despite all these setbacks, after several months, we were able to obtain active differentiated osteoclasts and we performed the experiments shown in our recent publication (8). We don't know the reason why finally we needed to maintain for 2 weeks the monocytes from PBMCs in flasks with M-CSF. Our hypothesis is that cells maybe need a rest time to stabilize in the flask, where there is more place for them. After that period, they are able to differentiate into osteoclasts with the addition of RANKL.

The possibility of observing the activity of osteoclasts on special bone surfaces was described in a few reports (9). The observation of resorbed areas in the Corning® Osteo Assay Surface Plates allows us to check the ability of the mature osteoclasts to resorb mineralized tissue. Although we have not shown these results, we performed a study in which we administrated substances that enhance or inhibit osteoclast activity, and the resorbed areas varied to a large extent. We intended to repeat these experiments several more times, but these plates were no longer manufactured.

In summary, we have established optimized conditions for osteoclast differentiation from both cell types: the RAW 264.7 murine cell line and from human monocytes. This experience will enable us and other researchers to carry out future studies with osteoclasts.

REFERENCES

1. Charles JF, Aliprantis AO. Osteoclasts: more than `bone eaters´.' Trends Mol Med 2014;20(8):449-59. DOI: 10.1016/j.molmed.2014.06.001
2. Khosla S. Minireview: The OPG/RANKL/RANK System. Endocrinology 2001;142(12):5050-5. DOI: 10.1210/endo.142.12.8536
3. Boyle WJ, Simonet WS, Lacey DL. Osteoclast differentiation and activation. Nature 2003;423(6937):337-42.
4. McDonald MM, Khoo WH, Ng PY, Xiao Y, Zamerli J, Thatcher P, et al. Osteoclasts recycle via osteomorphs during RANKL-stimu-

lated bone resorption. Cell 2021;184(5):1330-1347.e13. DOI: 10.1016/j.cell.2021.02.002
5. Nguyen J, Nohe A. Factors that Affect the Osteoclastogenesis of RAW264.7 Cells. J Biochem Anal Stud 2017;2(1):10.16966/2576-5833.109. DOI: 10.16966/2576-5833.109.
6. Song C, Yang X, Lei Y, Zhang Z, Smith W, Yan J, et al. Evaluation of efficacy on RANKL induced osteoclast from RAW264.7 cells. J Cell Physiol 2019;234(7):11969-75. DOI: 10.1002/jcp.27852
7. Abdallah D, Jourdain M-L, Braux J, Guillaume C, Gangloff SC, Jacquot J, et al. An Optimized Method to Generate Human Active Osteoclasts from Peripheral Blood Monocytes. Front Immunol 2018;9:632. DOI: 10.3389/fimmu.2018.00632
8. Jurado S, Parés A, Peris P, Combalia A, Monegal A, Guañabens N. Bilirubin increases viability and decreases osteoclast apoptosis contributing to osteoporosis in advanced liver diseases. Bone 2022;162:116483. DOI: 10.1016/j.bone.2022.116483
9. Wright LE, Buijs JT, Kim H-S, Coats LE, Scheidler AM, John SK, et al. Single-Limb Irradiation Induces Local and Systemic Bone Loss in a Murine Model. J Bone Miner Res 2015;30(7):1268-79. DOI: 10.1002/jbmr.2458

ROMM
Revista de Osteoporosis y Metabolismo Mineral

Original

Implication of connexins, integrins and primary cilium in bone cell activity

Sara Heredero-Jiménez, Irene Tirado-Cabrera, Eduardo Martín-Guerrero, Joan Pizarro-Gómez, Arancha R. Gortázar, Juan Antonio Ardura

Institute of Applied Medicine of the Universidad San Pablo-CEU. Madrid, Spain. Department of Basic Medical Sciences. School of Medicine. Universidad San Pablo-CEU. Madrid, Spain

Abstract

Background: osteocytes are capable of detecting different signals, transducing them into biological responses and transmitting them to osteoblasts and osteoclasts, allowing the maintenance of bone homeostasis. Bone mechanotransduction is possible because osteocytes have different mechanosensor structures such as connexins (Cxs), integrins, the primary cilium and even receptors coupled to G proteins such as the type 1 parathyroid hormone receptor (PTH1R).

Objective: to analyze the possible interaction of the different mechanosensor elements of the osteocytes and to observe their influence on the biological response.

Material and methods: we worked with the osteocytic cell lines MLO-Y4 Cx43+/+ (scrambled [SCR] and RNAi α2) and Cx43-/-.

Results and conclusion: our results show that Cx43 and integrin α2 are involved in lengthening the primary cilium, potentially affecting its functionality as a mechanosensor (SCR vs RNAi α2, $p < 0.0001$ SCR vs Cx43-/- and $p < 0.0001$ RNAi α2 vs Cx43-/-). The α2 integrin also influenced the cellular localization of Cx43, promoting its presence in the plasma membrane. Activation of PTH1R by agonists such as parathyroid hormone (PTH) and parathyroid hormone-related protein (PTHrP) was also found to induce ERK 1/2 kinase phosphorylation, and these effects could be affected by Cx43 deficiency, but do not appear to be. mediated by the silencing of α2 integrin. Finally, it was observed that the presence of Cx43 and integrin α2 in osteocytes increases their adhesion capacity (Cx43+/+ SCR and RNAi α2 vs CX43-/- $p < 0.001$ and $p = 0.0039$) and that deficiency in Cx43 causes an increase in the mortality of these cells (Cx43-/- vs Cx43+/+ $p = 0.0074$).

Keywords:
Osteocytes. Connexin 43. Primary cilium. Integrins. Mechanical stimulation. PTHrP.

Received: 18/07/2022 • Accepted: 13/10/2022

This article is sent in compliance with the commitment that was acquired upon obtaining the FEIOMM SCHOLARSHIP for Basic Research 2018.

Conflict of interest: the authors declare no conflict of interest.

Acknowledgments: we are grateful for the support of the Spanish Society of Bone and Mineral Metabolism (SEIOMM) and the Spanish Foundation for Bone and Mineral Metabolism Research (FEIOMM) that allowed us to prepare this manuscript.

Heredero-Jiménez S, Tirado-Cabrera I, Martín-Guerrero E, Pizarro-Gómez J, Gortázar AR, Ardura JA. Implication of connexins, integrins and primary cilium in bone cell activity. Rev Osteoporos Metab Miner 2023;15(1):12-20

DOI: 10.20960/RevOsteoporosMetabMiner.00006

Correspondence:
Juan Antonio Ardura. Institute of Applied Medicine of the Universidad San Pablo-CEU. Department of Basic Medical Sciences. School of Medicine. Universidad San Pablo-CEU. C/ Julián Romea, 23. 28003 Madrid, Spain
e-mail: juanantonio.ardurarodriguez@ceu.es

INTRODUCTION

Bone is a dynamic tissue that constantly remodels itself in response to a wide variety of stimuli, including hormones, growth factors and mechanical loading (1). Precise, coordinated control of bone remodeling requires interaction and communication between osteoblasts (bone-forming cells), osteocytes (main bone mechanosensor cells) and osteoclasts (cells responsible for bone resorption). It takes place, among other mechanisms, thanks to the formation of gap junctions (GJ) between these bone cells (2).

Osteocytes are capable of detecting mechanical stimuli due to the fact that they present different mechanosensory structures: integrins, GJ, connexin 43 hemichannels (Cx43), primary cilia and/or G protein-coupled receptors (GPCR), such as PTH1R3. Subsequently, these cells transduce the mechanical stimuli into biological responses, which trigger the activation of different signaling pathways, inducing changes in gene expression and cell metabolism. This causes the secretion of factors capable of regulating the proliferation and viability of bone effector cells (osteoblasts and osteoclasts). Due to the complexity of the extracellular environment of bone, it is very likely that the different mechanosensors interact with each other, integrating the multiple extracellular signals into a cohesive signal (4).

Cellular communication plays an important role in bone tissue, being embedded inside a mineralized matrix (5). Connexins (Cxs) are proteins that constitute some of the essential channels for communication between bone cells to take place.

Osteocytes may also promote bone formation due to the endocrine actions of PTH and its local analogue in bone, PTHrP, through the activation of PTH1R, their common receptor (6). PTH1R is a GPCR that can trigger various intracellular signaling pathways in bones (7).

The primary cilium is a mechanosensor structure capable of creating a different microdomain of the cell cytoplasm. This allows the specific location and concentration of receptors such as GPCRs, ion channels and effector proteins, thereby improving the kinetics of signaling pathways (8).

Various studies have shown that defects in the function or sensory structure of the primary cilium are associated with different diseases, generally referred to as ciliopathies (9). Likewise, when the formation of primary cilia is interrupted or their length decreases, the cells present an altered mechanosensitivity and a diminished response to mechanical stimulation (10).

Integrins are protein complexes that allow the cell to interact with the extracellular environment (11). Previous research has shown that in MLO-Y4 cells, β1 and α2 integrins are involved in the activation of extracellular signal-regulated kinases (ERK 1/2), induced by mechanical stimuli, which leads to the activation of signaling pathways that modulate the adhesion of osteocytes to the mineralized matrix and inhibit the apoptotic response of these cells (12).

In this study, we hypothesized the possible relationship between connexins, primary cilia, PTH1R and integrins as regulators of biological processes that would be crucial to the function of osteocytes.

MATERIALS AND METHODS

CELL CULTURE

Three types of MLO-Y4 cells Cx43+/+ (presenting an empty vector as a negative control to be able to evaluate the effects of non-silencing) and Cx43-/- (cells deficient in connexin 43, transfected with an RNAi) were used, which were kindly provided by Dr. L. I. Plotkin, and Cx43+/+ cells in which α2 integrin was silenced by RNAi. These cells were seeded at a concentration of 24,000 cells/cm^2 and cultured with α-Modified Eagle's Medium (α-MEM) (Gibco, ThermoFisher Scientific, ES) supplemented with 2.5 % calf serum (Calf Serum; CS), 2.5 % fetal bovine serum (Fetal Bovine Serum; FBS), 1 % L-glutamine, 1 % penicillin/streptomycin and Puromycin from *Streptomyces alboniger* (Sigma Aldrich, ES) at a concentration of 10 µg/ml.

All the surfaces on which these cells were seeded had to be previously collagenized with type I collagen at 0.01 % acetic acid13. Cells were kept at 37 °C and 5 % CO_2.

SILENCING OF α2 INTEGRIN

MLO-Y4 Cx43+/+ cells were transfected with three different α2 silencers (RNAi) (5 nM) (ThermoFisher Scientific, ES), targeting the α2 integrin sequence, using lipofectamine RNAiMax (Life Technologies, Carlsbad, CA, USA). The siRNAs were added in serum-free medium for 24 h. The scrambled sequence (SCR) (RNAi control, Santa Cruz Technology, TX, USA) was used as a negative control to evaluate the non-targeted effects of silencing (RNAi off-targeted).

PCR

RNA extraction was performed with TRIZOL® (Ambion, FosterCity, CA, USA). For RNA reverse transcription (RTPCR, reverse transcriptase polymerase chain reaction) the kit (Applied Byosistems, Grand Island, NY, USA) and the thermocycler (Eppendorf, Hamburg, Germany) were used.

To analyze the expression of the α2 integrin (Fw 5´CCATGATGGGTCGAAGCTGA3´; Rv 5´CTTCGTCGGCCACATTGAAA3´) SYBR Green (Sybr promix ex Taq, Takara, Otsu, Japan) was used. The level of α2 integrin expression was analyzed using β-actin as control gene (Fw 5´GAACCCTAAGGCCAACCGTG3´; Rv 5´ACCAGAGGCATACAGGGACAG3´). Triplicates of all conditions (Cx43+/+ and Cx43-/-) were performed. The expression change of the genes was calculated based on the value of $2^{-\Delta\Delta Ct}$.

IMMUNOFLUORESCENCE

Multiwell plates (Falcon, ES) were seeded at 30,000 cells/well. Cells were grown until they reached 80 % confluency and serum-free medium was added for 24 h to induce primary cilium formation. Cells were then fixed with 4 % paraformaldehyde (PFA) and permeabilized with 0.5 % Triton X-100. Next, the blocking solution composed of 10 % bovine serum albumin (BSA), supplemented with 5 % goat serum, was added for 1 h. Subsequently, the following primary antibodies were kept overnight at 4 °C under agitation: polyclonal anti-Cx43 produced in rabbit (Sigma, ST. Louis, MO, USA) (1:1000 dilution in 10 % BSA and 5 % goat serum); and mouse monoclonal acetylated anti-α tubulin (Sigma) (1:1000 dilution in 10 % BSA and 5 % goat serum), to observe the primary cilium. Secondary antibodies were then added: Alexa fluor® 488 goat anti-mouse primary cilia (Invitrogen Molecular probes, Thermo Fisher ScientificTM, ES) (1:1000 dilution in 10 % BSA and 5 % goat serum), to Cx43 Alexa fluor® 568 anti-rabbit IgG (Live technologies, Thermo Scientific™, ES) (1:1000 dilution in 10 % BSA and 5 % goat serum). After 1 h of incubation, 4'-6-diamidino2-phenylindole (DAPI) (1:10,000 dilution) was added. The nuclei, the primary cilium and the Cx43 were visualized with the epifluorescence microscope (Leica CTR 6000). Triplicates were imaged and a total of 100 cells from each condition (Cx43+/+ SCR and α2 and Cx43-/-) were analyzed. The fusion of the individual images of the primary cilium, Cx43 and cell nuclei into one was performed with the ImageJ program, which allows processing digital images, is capable of calculating the area and the statistics of the value of the pixel selected by the user and to measure distances.

STIMULATION BY PTH1R AGONISTS (PTH AND PTHrP)

To perform stimulation by PTHrP and PTH, cells were plated at a density of 25,000 cells/cm^2 and both ligands were added at a concentration of 10-7 molar (M), for 10 min.

CELL DEATH AND ADHESION ASSAY

Cell viability was determined by trypan blue exclusion, a method that stains dead cells blue, allowing the percentage of live and dead cells to be calculated with respect to the total using a Neubauer camera and a bright field optical microscope (Leica DM5500B). to do the counting.

After trypsinizing the cells and 30 minutes after reseeding, non-adherent cells were counted with the Neubauer chamber. Next, images of different fields of the cells adhered to the Petri dish were taken, using an inverted bright field microscope (Leica DM5500B), to calculate the percentages of cells adhered to the total. A total of 9 fields of each condition were analyzed in triplicate (Cx43+/+ SCR and α2 and Cx43-/-).

WESTERN BLOT ANALYSIS

Protein extraction was performed for each condition in duplicate (Cx43+/+ SCR and α2 and Cx43-/-), using RIPA Buffer (150 mM NaCl, 1.0 % IGEPAL® CA-630, 0.1 % SDS (sodium dodecyl sulfate), 50 mM Tris, pH 8, Sigma-Aldrich, St Louis, MO, USA), protease inhibitor (PI) (1:100 dilution, Calbiochem®, ES) and phosphatase inhibitor (IF) (1:100 dilution, Calbiochem®, IT IS). Proteins were quantified by the bicinchoninic acid (BCA) assay (Pierce™ BCA Protein Assay Kit, Thermo Fisher Scientific, ES). To carry out the reading, the Variouskan Flash plate reader (Thermo Fisher Scientific, ES) was used and three readings were made at 562 nm using the SkanIt Software 2.4.3 RE program.

Protein extracts were separated using a polyacrylamide gel. Proteins were subsequently transferred to a nitrocellulose membrane (Bio-Rad, Hercules, CA, USA). The blocking was carried out with 5 % milk powder in Tris saline buffer with Tween20 (TTBS) at 0.05 %, for 1 h under stirring at room temperature. Next, the following primary antibodies were incubated for 24 hours at 4 °C and under agitation: anti-phospho-p44/42 MAPK (Erk 1/2) (Cell Signaling, Beverly, MA, USA), anti-p44/42 MAPK (Erk 1/2), and anti-α-tubulin (Sigma Aldrich, ES). Subsequently, secondary antibodies were added. Chemiluminescence development was carried out with Clarity™ Western ECL substrate (Bio-Rad). The intensity of the bands was quantified by densitometry, using Dnr Bio Imaging System MF ChemiBIS3.2 and the programs Gelcapture and QuantityOneTM (Bio-Rad).

STATISTICAL ANALYSIS

The confidence limit established in all the statistical tests was 95 %. Therefore, results with a p value (p) $p < 0.05$ are considered statistically significant.

For the comparison of means ± standard deviation (SD), the GraphPad Prism 8 program was used. To compare means of more than two groups, the ANOVA test of a single factor and the ANOVA Welch test were used. Equality of variances was not considered. For multiple analyses, Dunnett's test, Tukey's test and the non-parametric Kruskal Wallis test were used. Being t the statistic that analyzes if the measures of the two conditions are equal or not and gl that would be the degrees of freedom that indicate the number of values that can be assigned arbitrarily.

RESULTS

INTEGRIN GENE EXPRESSION MODULATED BY CONNEXIN 43 IN OSTEOCYTIC CELLS

The RNA expression of integrins α2, α6, β1, β3 and β6 and Cx43 was analyzed by means of quantitative PCR, to study the possible relationship in the expression of these two families of proteins.

Figure 1 shows how the α2 integrin significantly decreases its expression level in cells of the Cx43-/- line compared to Cx43+/+ cells (t = 13.93, gl = 4, $p = 0.0002$). On the contrary, the α6, β1 and β3 integrins significantly increase their expression in the Cx43-/- cell line compared to Cx43+/+ (t = 3.646, df = 4, $p = 0.0219$; t = 5.501, g = 4, $p = 0.0053$, t = 26.18, gl = 4, $p < 0.0001$, respectively). In the case of β6, no significant differences were observed between the two cell lines (t = 0.99, df = 4, $p = 0.378$).

These results indicate that the expression of connexin 43 conditions the expression pattern of various integrins in osteocytic cells.

CONNEXIN 43 AND INTEGRIN α2 REGULATE THE LENGTH OF THE PRIMARY CILIUM IN OSTEOCYTIC CELLS

Immunofluorescence was performed to observe the possible relationship and interaction between the primary cilium, Cx43 and α2 integrin, three well-known mechanosensors of osteocytes, and to determine if the development and length of the primary cilium could depend on the presence of Cx43 and α2 integrin (Fig. 2).

MLO-Y4 Cx43+/+, MLO-Y4 Cx43+/+ cells silenced with α2 integrin (RNAi α2), and MLO-Y4 Cx43-/- cells were compared. In the results shown in figure 3, it was observed that all cell lines are capable of developing primary cilium and that this organelle originates on the cell surface. In addition, it was observed that Cx43 presents a different distribution in Cx43+/+ and α2 RNAi cells, since in cells in which the α2 integrin was not silenced, the presence of Cx43 predominates in the cell membrane, an expected location, since it is where it forms hemichannels and UCs. While in the conditions in which the cells do not present α2 integrin, Cx43 is distributed in the cell cytoplasm and not so focused on the plasma membrane. Immunofluorescence images also showed that Cx43 and the primary cilium do not co-localize.

In order to quantitatively compare the development of the primary cilium and its length, images of each cell type (Cx43+/+ SCR, Cx43+/+ RNAi α2 and Cx43-/-) were analyzed. These images were taken from different fields using fluorescence microscopy (40X).

Statistical analyzes were carried out comparing the means ± SD of the length in μm of all the cilia analyzed in the cells Cx43+/+ SCR (2.37), Cx43+/+ RNAi α2 (2.08) and Cx43-/- (1.52). The results obtained indicate that the length of the primary cilium in cells in which α2 integrin was silenced and in cells deficient in Cx43 was significantly less than in scrambled cells. The p-value was: $p = 0.0017$ for the comparison of SCR vs RNAi α2, $p < 0.0001$ SCR vs Cx43-/- and $p < 0.0001$ RNAi α2 vs Cx43-/- (Fig. 3).

Based on these observations, we can suggest that connexin 43 and integrin α2 are involved in primary ciliary elongation in osteocytic cells.

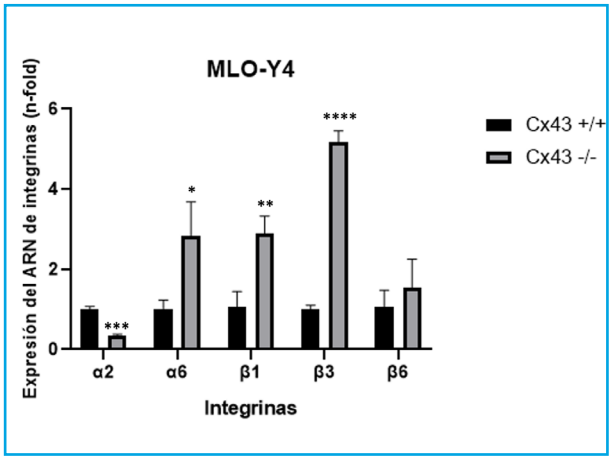

Figure 1. RNA expression of integrins α2, α6, β1, β3 and β6 in Cx43 +/+ and Cx43-/- cells. The results are expressed as mean ± SD of an experiment performing triplicates of each experimental condition *$p < 0.05$; **$p < 0.01$; ***$p < 0.001$; ****$p < 0.0001$.

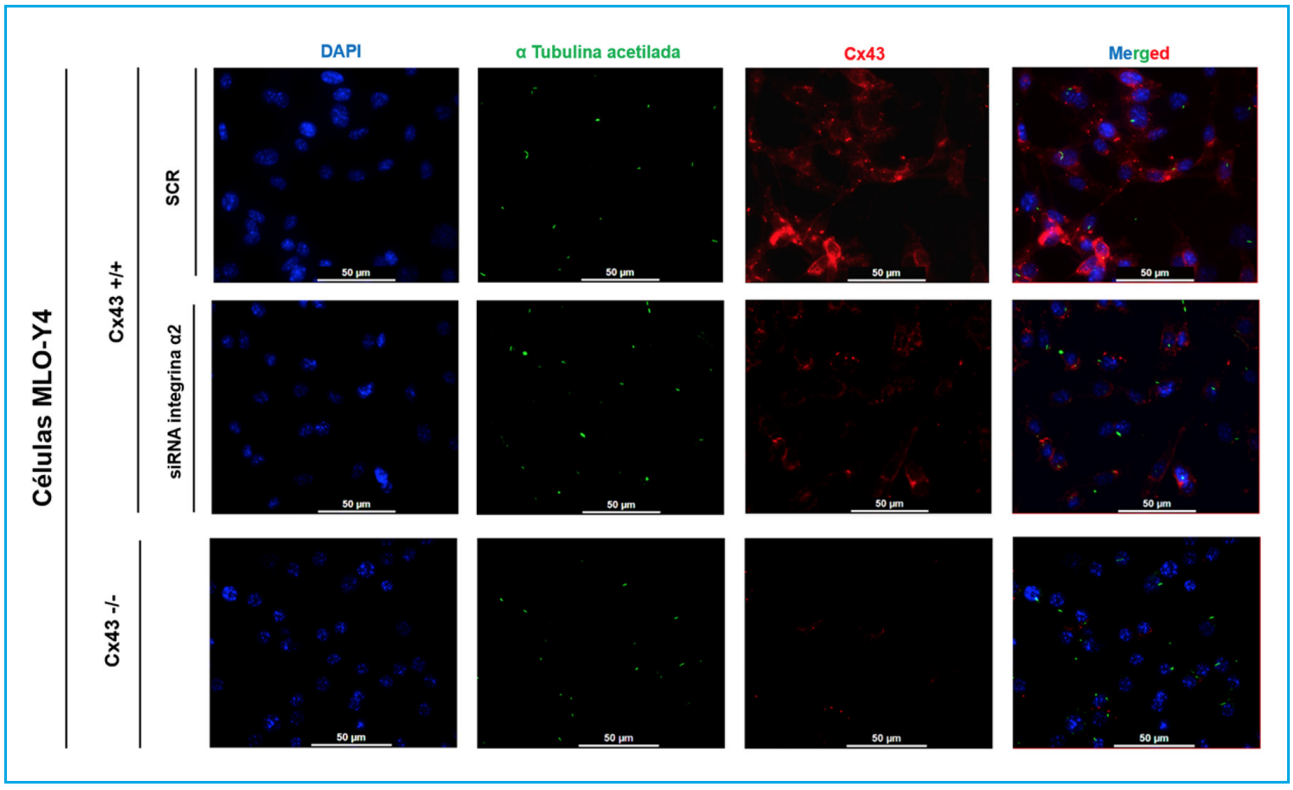

Figure 2. Immunofluorescence of MLO-Y4 Cx43+/+ (SCR and RNA α2) and Cx43 -/- cells. The cell nucleus was visualized with DAPI (blue), the primary cilium with the anti-α-acetylated tubulin antibody (green) and the Cx43 with the anti-Cx43 antibody (red). Images were captured with a confocal fluorescence microscope (40X). Scale bar = 50 µm.

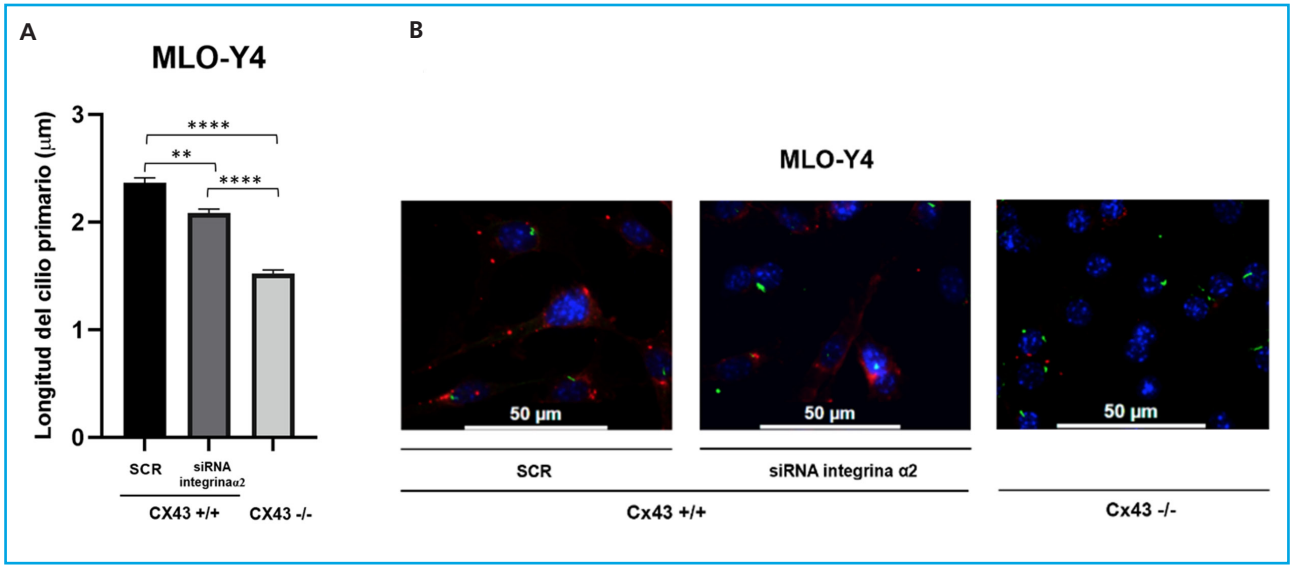

Figure 3. Comparison of primary cilium length (µm) between lines Cx43+/+ (SCR and RNAi α2) and Cx43-/-. A. The results show the mean value ± SD of the length of the primary cilium in mean µm from the images made at different fields. *$p < 0.05$; **$p < 0.01$; ***$p < 0.001$; ****$p < 0.0001$. B. Representative images in which the nucleus can be visualized by DAPI (blue) and the primary cilium by anti-α-acetylated tubulin antibody (green). The images were captured with a confocal fluorescence microscope (40X). Scale bar = 50 µm.

REGULATION OF ERK KINASE 1/2 PHOSPHORYLATION BY CONNEXIN 43 IN OSTEOCYTIC CELLS

To characterize the response of MLO-Y4 cells (Cx43+/+ and Cx43-/-) to stimulation by agonists, the PTH1R, PTH and PTHrP (1-37) receptor ligands were added to the culture medium at a concentration of 10^{-7} M, for 10 min. Immediately afterwards, protein extraction was performed to analyze P-ERK expression by Western blot. The purpose of this experiment was to determine if Cx43 deficiency influenced the activation of the PTH1R receptor after stimulating it with their respective ligands (PTH and PTHrP) and to analyze the intracellular signaling pathways that this stimulus activates and the cellular response that it triggers, specifically the ERK 1/2 phosphorylation.

The results obtained show that in Cx43+/+ cells, stimulation with PTH and PTHrP increases ERK 1/2 phosphorylation (mean ± SD of the duplicates made) with respect to cells that were not stimulated with any ligand (CE). In the case of Cx43-/- cells, PTH stimulation decreased ERK phosphorylation relative to Cx43+/+ cells that were stimulated with PTH, and the agonist peptide PTHrP did not stimulate Cx43-/- cells. No significant variations were obtained in the levels of P-ERK between the different experimental conditions (Fig. 4).

Our observations suggest that connexin 43 regulates ligand-activated PTH1R-dependent phosphorylation of ERK 1/2.

Cx43 EXPRESSION REGULATES VIABILITY AND ADHESION OF OSTEOCYTIC CELLS

A cell death assay was performed with Cx43+/+ SCR, RNAi α2 and Cx43-/- cells in order to determine whether the lack of expression of integrin α2 and Cx43 would modify the signaling pathways involved in the cell response, causing its apoptosis. Figure 5A shows how the number of live Cx43-/- cells decreases significantly with respect to Cx43+/+ SCR cells (p = 0.0035). In the case of the analysis of dead cells, we see that their number increases significantly in Cx43-/- cells compared to Cx43+/+ SCR (p = 0.0074).

As for the Cx43+/+ RNAi α2 cell line, as there were no significant differences in the number of live cells (although there was a slight tendency towards a decrease in their number) and it presented a very similar number of dead cells with respect to cells. Cx43+/+ SCR, it is suggested that the silencing of the α2 integrin influences the proliferation of osteocytes and not their death.

On the other hand, an adhesion assay was also performed on Cx43+/+ SCR, RNAi α2 and Cx43-/- cells. Figure 5B shows that the number of Cx43-/- cells adhered to the collagen plaque decreases significantly with respect to Cx43+/+ SCR and α2 RNAi cells (p < 0.001 and p = 0.0039, respectively). In the case of counting non-adherent cells, their number increased significantly both in Cx43+/+ RNAi α2 cells and in Cx43-/- compared to Cx43+/+ SCR (p = 0.0146 and p = 0.0134, respectively).

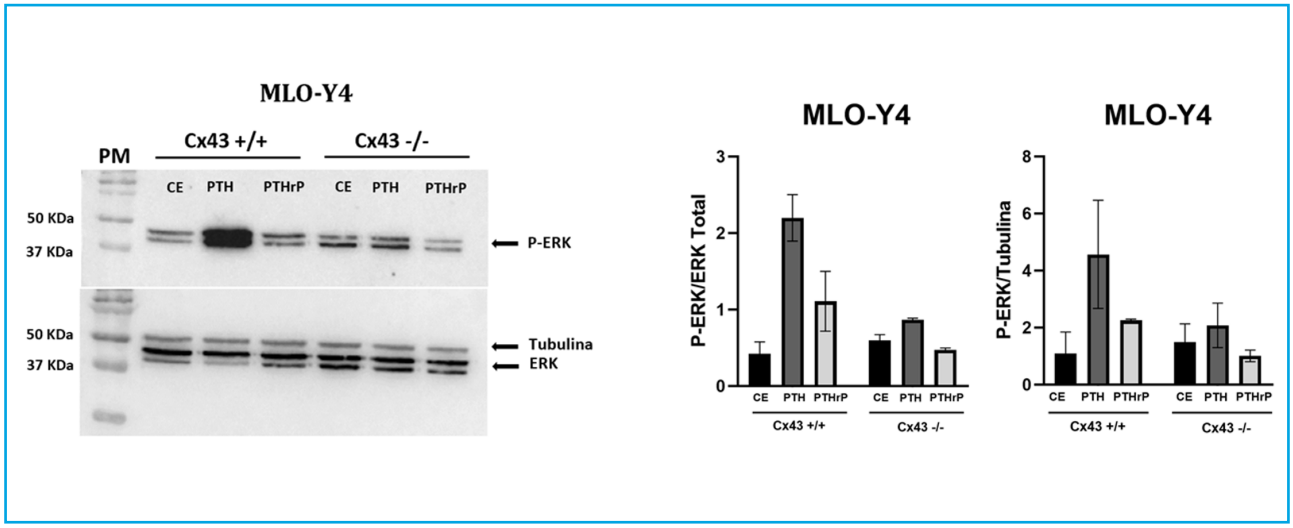

Figure 4. Analysis of P-ERK after stimulating MLO-Y4 Cx43+/+ and Cx43-/- cells with PTH and PTHrP. In Cx43+/+ cells, stimulation with PTH and PTHrP increases ERK 1/2 phosphorylation vs. cells that were not stimulated with any ligand (CE) (2.200 ± 0.696 vs. 0.4240 ± 0.150 and 1.11 ± 0.554 vs. to 0.4240 ± 0.150, respectively). In Cx43-/- cells, PTH stimulation decreased ERK phosphorylation relative to Cx43+/+ cells that were stimulated with PTH (0.865 ± 0.003 vs. 2.20 ± 0.696). Total ERK and tubulin values were used to normalize P-ERK values. Results are expressed as mean ± SD of a duplicate experiment of each experimental condition vs. CE.

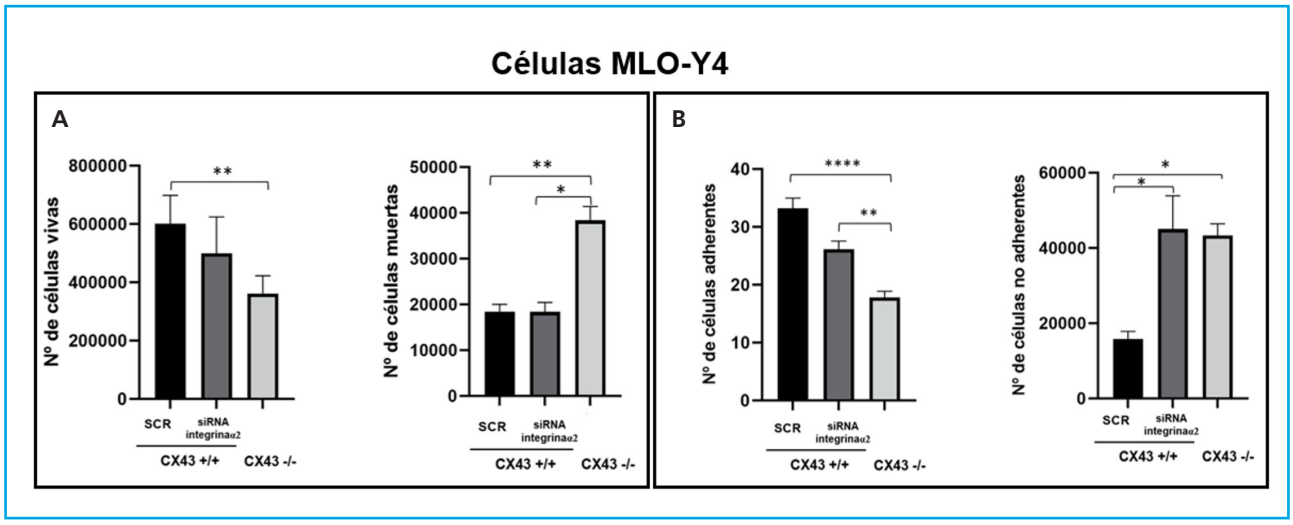

Figure 5. Analysis of cell death (A) and cell adhesion (B) in Cx43+/+ (SCR and α2 ARNi) and Cx43-/- cells. The results show the mean ± SD values of live and dead cell counts from a single experiment with six replicates for each condition, and the counts of adhered and non-adhered cells on the plate. *$p < 0.05$; **$p < 0.01$; ***$p < 0.001$; ****$p < 0.0001$.

Cell adhesion was quantified using brightfield images, which also allowed the morphology of the different cell types to be analyzed, and it was observed that the Cx43+/+ SCR cells had a more elongated shape and a greater number of dendritic extensions, which would potentially allow them to have a higher adhesion capacity. In contrast, Cx43+/+ RNAi α2 and Cx43-/- cells showed a more rounded structure, probably due to the absence of both integrins and connexins, both transmembrane proteins that favor cell adhesion (4).

These results are related to those obtained in the cell death assay, since we observed a greater number of dead cells in the Cx43-/-, due to the lack of Cx43, adhesion to the culture surface would be difficult, which could cause cells to detach and die due to lack of substrate binding.

DISCUSSION

Integrins and connexins play an essential role in cellular functions (14). However, it has not been clarified whether the interaction of both families of proteins is necessary for the proper functioning of osteocytes. The decrease in α2 integrin expression in the Cx43-/- cells led us to consider whether this integrin could act as a mediator in the processes dependent on Cx43 in the osteocytes.

In addition to Cxs and integrins, the primary cilium is also considered a mechanosensor of osteocytes (4). In the immunofluorescence images, it was possible to observe how the deficiency in Cx43 and the silencing of the integrin α2 influence the length of the primary cilium. Various studies indicate that the length of the primary cilium is a determining factor for its correct action as a mechanosensory (4), given that if the length of the cilium is very small, the space of the ciliary membrane would decrease where ion channels and receptors such as PTH1R that mediate the ciliary membrane detected by the cilium and allow the transduction of different intracellular signals (15). Furthermore, the primary cilium generates a specific intracellular compartment in which the intra-flagellar transport of different proteins is necessary both for the development of this organelle and for signal transduction (16). Therefore, if this space is reduced, these processes could be altered, causing the osteocytes not to generate adequate responses to extracellular stimuli (10).

In the immunofluorescence images, a different distribution of Cx43 between Cx43+/+ SCR and Cx43+/+ RNAi α2 cells also seems to be observed. Although in both conditions the expression levels of Cx43 are similar, that is, the silencing of the integrin α2 did not influence the expression of Cx43, it could influence the cellular localization of this protein, since in the Cx43+/+ cells the Cx43 It was found mainly in the cell membrane. These results could indicate that integrin α2 and Cx43 interact in the cell membrane and that their expression triggers a positive feedback favoring the transport of these proteins from the endoplasmic reticulum to the cell membrane.

The osteocytes, embedded in the mineralized matrix, are capable of detecting different signals, translating them into biological responses and transmitting them to the rest of the bone cells, mainly osteoblasts and osteoclasts, to allow the maintenance of bone homeostasis (17). One of these signals is stimulation by PTH1R agonists (PTHrP and PTH) (18).

Our results indicate that ERK 1/2 phosphorylation increases in Cx43+/+ cells when they are stimulated with PTH and PTHrP. In the case of Cx43-/- cells, stimulation with PTH and PTHrP seems to be inhibited since the levels of phospho-ERK 1/2 decrease with respect to Cx43+/+ cells. This may be due to the fact that Cx43-/- osteocytes are less sensitive to stimuli, given that they are deficient in the Cx43 protein that acts as a mechanosensory and also have a shorter primary cilium. All this would cause the PTH1R to have less space to locate itself in the ciliary membrane and generate intracellular responses such as the phosphorylation of ERK 1/2. Another of the results observed in this experiment is that it seems that the increase in ERK 1/2 phosphorylation is greater when we stimulate with PTH than with PTHrP, at the time studied (10 min), which would indicate that both agonists activate PTH1R differently. This activation mechanism is probably mediated by Cx43. However, more experiments would be required to confirm that this stimulation can generate a modification in ERK phosphorylation and therefore a biological response in the cell.

Other characteristics analyzed in these cells were their morphology, adhesion capacity and cell death. The Cx43+/+ SCR cells were found to have a more elongated shape and a greater number of dendritic extensions, which increased their adhesion capacity. In contrast, Cx43+/+ RNAiα2 and Cx43-/- cells have a more rounded morphology and a lower adhesion capacity compared to Cx43+/+ SCR cells. Cx43-/- cells also show a higher mortality compared to the other two cell types. Based on these results, it is suggested that the absence of Cx43 and integrin α2 prevent the correct adhesion of cells to the collagenized plate, which in turn would compromise the development of dendritic extensions (19). Reducing the number of dendritic extensions would cause the communication between cells to be altered and since this communication is essential for cell survival, it could explain why a higher mortality is observed in Cx43-/- cells. The results obtained concur with previous research in which it has been shown that connexins and integrins are proteins that intervene in cell adhesion (20). In addition, Cx43 regulates different signaling pathways that lead to the expression of pro-survival genes21, which is consistent with the results observed. In the case of Cx43+/+ RNAi α2 cells, alterations in cell adhesiveness could cause less pronounced cellular effects, since no alterations in cell survival were observed under these conditions. However, the decrease in adhesiveness could explain the tendency of these cells to proliferate less than Cx43+/+ SCR.

CONCLUSION

Our study indicates that Cx43 deficiency modifies the expression pattern of integrins in MLO-Y4 osteocytes, inhibiting the expression of integrin α2 and increasing that of integrins α6, β1 and β3, which seems to modify their adhesion capacity. In addition, the absence of integrin α2 and Cx43 alters the length of the primary cilium.

REFERENCES

1. Scheuren A, Wehrle E, Flohr F. Bone mechanobiology in mice: toward single-cell in vivo mechanomics. Biomech Model Mechanobiol 2017;16(1):2017-34. DOI: 10.1007/s10237-017-0935-1
2. Claude J. Membrane channels formed by gap junction proteins. Biochim Biophys Acta Biomembr 2018;1860(1):1-4. DOI: 10.1016/j.bbamem.2017.10.021
3. Rupp M. Osteocytes. Z Orthop Unfall 2019;157(02):154-63. DOI: 10.1055/a-0658-5922
4. Geoghegan IP, Hoey DA, McNamara LM. Integrins in Osteocyte Biology and Mechanotransduction. Curr Osteoporos Rep 2019;17(4):195-206. DOI: 10.1007/s11914-019-00520-2
5. Plotkin LI, Davis HM, Cisterna BA, Sáez JC. Connexins and Pannexins in Bone and Skeletal Muscle. Curr Osteoporos Rep 2017;15(4):326-34. DOI: 10.1007/s11914-017-0374-z
6. Esbrit P, Alcaraz MJ. Current perspectives on parathyroid hormone (PTH) and PTH-related protein (PTHrP) as bone anabolic therapies. Biochem Pharmacol 2013;85(1):1417-23. DOI: 10.1016/j.bcp.2013.03.002
7. Ardura JA, Portal-Núñez S, Alonso V, Bravo B, Gortázar AR. Handling parathormone receptor type 1 in skeletal diseases: Realities and expectations of abaloparatide. Endocrinol Metab 2019;30(10):756-66. DOI: 10.1016/j.tem.2019.07.014
8. Hoey DA, Downs ME, Jacobs CR. The mechanics of the primary cilium: an intricate structure with complex function. J Biomech 2012;45(1):17-26. DOI: 10.1016/j.jbiomech.2011.08.008
9. Mirvis M, Stearns T, James W. Cilium structure, assembly, and disassembly regulated by the cytoskeleton. J Biochem 2018;475(14):2329-53. DOI: 10.1042/BCJ20170453
10. Pala R, Alomari N, Nauli SM. Primary Cilium-Dependent Signaling Mechanisms. Int J Mol Sci 2017;18(11):2272-345. DOI: 10.3390/ijms18112272
11. Batra N, Burra S, Siller-Jackson AJ, Gu S, Xia X, Weber GF, et al. Mechanical stress-activated integrin α5β1 induces opening of connexin 43 hemichannels. PNAS 2012;109(9):3359-64. DOI: 10.1073/pnas.1115967109
12. Plotkin LI, Mathov I, Aguirre JI. Mechanical stimulation prevents osteocyte apoptosis: requirement of integrins, Src kinases and ERKs. Am J Physiol Cell Physiol 2005;289(3):633-43. DOI: 10.1152/ajpcell.00278.2004
13. Kato Y, Windle JJ, Koop BA, Mundy GR, Bonewald LF. Establishment of an Osteocyte- like Cell Line, MLO-Y4. J Bone Miner Res 1997;12(12):2014-23. DOI: 10.1359/jbmr.1997.12.12.2014
14. Plotkin LI, Speacht TL, Donahue HJ. Cx43 and mechanotransduction in bone. Curr Osteoporos Rep 2015;13(2):67-72. DOI: 10.1007/s11914-015-0255-2
15. Martín-Guerrero E, Tirado-Cabrera I, Buendía I, Alonso V, Gortázar AR, Ardura JA. Primary cilia mediate parathyroid hormone receptor type 1 osteogenic actions in osteocytes and osteoblasts via Gli activation. J Cell Physiol 2020;235(10):7356-69. DOI: 10.1002/jcp.29636
16. Zhang J, Chandrasekaran G, Li W, Kim DY, Jeong IY, Lee SH, et al. Wnt-PLC-IP3-Connexin-Ca2+ axis maintains ependymal motile cilia in zebrafish spinal cord. Nat Commun 2020;11(1):1860. DOI: 10.1038/s41467-020-15248-2
17. Cresswell EN, Nguyen TM, Horsfield MW, Alepuz AJ, Metzger TA, Niebur GL, et al. Mechanically induced bone formation is not sensitive to local osteocyte density in rat vertebral can-

cellous bone. J Orthop Res 2018;36(2):672-81. DOI: 10.1002/jor.23606
18. Tirado-Cabrera I, Martin-Guerrero E, Heredero-Jimenez S, Ardura JA, Gortázar AR. PTH1R traslocation to primary cilia in mechanically-stimulated osteocytes prevents osteoclast formation via regulation of CXCL5 and IL-6 secretion. J Cell Physiol 2022;237(10):3927-43. DOI: 10.1002/jcp.30849
19. Rolvien T, Amling M. Disuse Osteoporosis: Clinical and Mechanistic Insights. Calcif Tissue Int 2022;110(5):592-604. DOI: 10.1007/s00223-021-00836-1
20. Cheng B, Zhao S, Luo J, Sprague E, Bonewald LF, Jiang JX. Expression of Functional Gap Junctions and Regulation by Fluid Flow in Osteocyte-Like MLO-Y4 Cells. J Bone Miner Res 2001;16(2):249-59. DOI: 10.1359/jbmr.2001.16.2.249
21. Gortazar AR, Martin-Millan M, Bravo B, Plotkin LI, Bellido T. Crosstalk between caveolin-1/extracellular signal-regulated kinase (ERK) and β-catenin survival pathways in osteocyte mechanotransduction. J Biol Chem 2013;288(12):8168-75. DOI: 10.1074/jbc.M112.437921

ARÁN

ROMM
Revista de Osteoporosis y Metabolismo Mineral

Original

The secretome of mechanically stimulated osteocytes modulates mesenchymal cell function

Álvaro Tablado Molinera, Irene Gutiérrez Rojas, Luis Álvarez Carrión, Irene Tirado Cabrera, Sara Heredero-Jiménez, Arancha R. Gortázar, Juan Antonio Ardura

Institute of Applied Medicine of the Universidad San Pablo-CEU. Madrid, Spain. Department of Basic Medical Sciences. School of Medicine. Universidad San Pablo-CEU. CEU Universities. Madrid, Spain

Abstract

The skeleton is a metabolically active organ that is continuously remodeled throughout our lives. This remodeling entails a balance between the formation of bone conducted by the osteoblasts and resorption by osteoclasts. Osteocytes regulate these two processes and their mechanical stimulation is essential to maintain the good functioning of bones and prevent diseases such as osteoporosis. Osteocyte stimulation causes an alteration in the production and secretion of signaling molecules that regulate osteoblast and osteoclast activity. Mesenchymal stem cells have been proposed as a possible cellular therapy for the regeneration of different tissues including bone tissue. We hypothesize in the present study that the secretome of mechanically stimulated osteocytic mouse cells affect the proliferative, adhesive capacity and gene expression of undifferentiated mesenchymal cells and preosteoblastic mesenchymal cells. To that end, the above-mentioned biological processes were analyzed in continuous preosteoblastic cellular lines and mouse mesenchymal cells in the presence of the medium conditioned by MLO-Y4 osteocytic cells after undergoing a mechanical stimulus by fluid flow. It was observed that proliferation increased in both cellular lines in the presence of secretome of mechanically stimulated osteocytes versus control while non-mechanically stimulated osteocytes caused its reduction. It was also possible to observe an increased adhesive capacity of C3H/10T1/2 cells after stimulation with the secretome of mechanically stimulated osteocytes. Regarding gene expression, only the adipogenic factor PPARγ underwent alterations in MC3T3-E1 cells by the secretome of osteocytes. These studies indicate that osteocytes can modify the biological behavior of mesenchymal cells by the secretion of soluble factors.

Keywords:
Mechanical stimulus.
Osteocytes.
Mesenchymal cells.
Mechanotransduction.

Received: 22/07/2022 • Accepted: 27/02/2023

Conflicts of interest: the authors declare no conflict of interest.

Acknowledgements: we wish to thank the support given from the Spanish Society for Bone Research and Mineral Metabolism (SEIOMM) and the Spanish Foundation for Bone and Mineral Metabolism Research (FEIOMM) for making this manuscript possible.

Tablado Molinera A, Gutiérrez Rojas I, Álvarez Carrión L, Tirado Cabrera I, Heredero-Jiménez S, Gortázar AR, Ardura JA. The secretome of mechanically stimulated osteocytes modulates mesenchymal cell function. Rev Osteoporos Metab Miner 2023;15(1):21-28

DOI: 10.20960/RevOsteoporosMetabMiner.00007

Correspondence:
Juan Antonio Ardura. Institute of Applied Medicine the Universidad San Pablo-CEU. Madrid. Department of Basic Medical Sciences. School of Medicine. Universidad San Pablo-CEU. CEU Universities.
C/ Julián Romea, 23. 28003 Madrid, Spain
e-mail: juanantonio.ardurarodriguez@ceu.es

INTRODUCTION

The skeleton is a metabolically active organ that is continuously remodeled throughout our lives. The bone remodeling process, in which bone matrix resorption and formation are coupled, serves the purpose of adjusting bone architecture to the mechanical needs of the bone. In addition, it helps repair damage to the bone matrix and prevent the accumulation of old bone that may have lost its mechanical properties (1).

There are many factors that modulate the formation and maintenance of our skeleton. Among them, mechanical load represents the main extrinsic factor with direct effects on bone tissue (2). Load on our bones translates into mechanical tensions that are received by bone cells and transformed into biological signals, which is known as mechanotransduction (2).

Osteoblasts and osteoclasts are the cells involved in bone formation and resorption, respectively (3). Osteocytes, the most abundant bone tissue cells of all, are the main receptors of mechanical stimulation and capable of communicating with osteoblasts and osteoclasts by modulating their activity (4).

Bone cells are in close contact with the cells present in the bone marrow. There we find a very heterogeneous cell population where hematopoietic cells coexist giving rise to different blood populations with the bone marrow microenvironment for non-hematopoietic cells such as perivascular and mesenchymal cells (MSC) among others (5).

The MSC present in the marrow are the source of osteoprogenitor cells that make it possible for fractures to be repaired and new bone to be formed (5).

The differentiation of mesenchymal stem cells is a process that consists of 2 stages; commitment to a cellular lineage (from the MSC to a progenitor of a specific lineage) and maturation (from progenitors to a specific cellular type). A large number of signaling pathways are involved in the regulation of MSC lineage commitment, among which we can find the TGF-beta family, BMP (bone morphogenic proteins), Wnt, hedgehogs (Hh), Notch, and fibroblast growth factors (FGF) (6,7).

In this article we study the communication between osteocytes and mesenchymal cells, and how mechanical stimulation modifies the proliferation, adhesion and gene expression of mesenchymal cells through osteocytes.

We hypothesized that the secretome of mechanically stimulated osteocytes induces biological processes related with the strengthening of bone regeneration capabilities of mesenchymal cells, and for that purpose we have studied the effect of the medium conditioned by mechanically stimulated MLO-Y4 osteocytes (by fluid flow) or not (static control) on different biological processes of C3H/10T1/2 mesenchymal and MC3T3-E1 preosteoblastic cells.

MATERIAL AND METHODS

CELL CULTURES

The following cellular lines were used for the assays of the present work: mouse mesenchymal cells uncommitted to osteoblastic lineage (C3H/10T1/2 subclone 8, ATTC, CCL-226). These cells were cultured with BME medium ("basal eagle medium," Thermofisher, 21010046) + 10 % fetal bovine serum (FBS) (Thermofisher, 10500064) + 1 % L-glutamine (Thermofisher, 25030024) + 1 % penicillin/streptomycin (Thermofisher, 15140122) at 37 °C with 5 % of CO_2. Mouse preosteoblastic mesenchymal cells (MC3T3-E1 subclone 4, ATTC, CRL-2593). These cells were cultured with MEM alpha medium ("minimum essential medium," Thermofisher, A1049001) + 10 % FBS + 1 % L-glutamine and 1 % streptomycin/penicillin at 37 °C with 5 % of CO_2. Murine MLO-Y4 osteocytic cells (Kerafast, EKC002). These cells were cultured with MEM alpha medium without ascorbic acid (Thermofisher, 22571038) + 2.5 % FBS + 2.5 % of calf serum ("calf serum" [CS], Thermofisher, 16010159) and 1 % streptomycin/ penicillin at 37 °C with 5 % of CO_2.

MECHANICAL STIMULATION BY FLUID FLOW

A collection of 250 000 MLO-Y4 cells were seeded on Teflon-coated glass slides in a 15 cm^2 area previously covered with a collagen matrix (Sigma Aldrich, 000010C8919). After 48 hours, the cells unerwent a mechanical stimulus (FF) using the Flexcell Streamer fluid shear stress device that produces a stress of 10 dynes/cm^2 for 10 minutes (Flexcell International Corporation, Hillsborough, North Carolina, USA). As static control or SC, MLO-Y4 cells were seeded on a Teflon-coated glass slide without undergoing any mechanical stimulus. Afterwards, the cells were incubated for 18 hours, with MEM alpha medium without phenol red (Gibco) supplemented with 0.5 % of CS, 0.5 % of FBS, and 1 % of penicillin-streptomycin to obtain conditioned media (CM) of the different experimental groups: mechanostimulated cells (FF) and control cells.

PROLIFERATION ASSAY

To conduct proliferation assays, both MC3T3-E1 and C3H/10T1/2 cell lines were seeded at a density of 20 000 cells/well in 24-well culture microplates (VWR,734-2325). The following day the medium was changed for a medium with 250 µl of conditioned medium (static control or fluid flow) and 750 µl of its corresponding culture medium. MC3T3-E1 and C3H/10T1/2 cells were used as control incubated

with 250 µL of MEM alpha without phenol red (Gibco) supplemented with 0.5 % of CS, 0.5 % of FBS, 1 % of penicillin-streptomycin, and 750 µl of its corresponding culture medium. After 24 h of incubation the cells were detached with Trypsin-EDTA (Thermofisher, 25300062) and cell count started with Trypan blue (Thermofisher, 15250061) in Neubauer chamber. The same process was repeated at 48, 72 and 96 hours and assessment of the proliferation was obtained.

CELL ADHESION

Adhesion of MC3T3-E1 preosteoblastic cells and C3H/10T1/2 mesenchymal cells was evaluated by cell quantification of marked with vital fluorescent dye cytopainter (Abcam, ab176735). To that end, MC3T3-E1 or C3H/10T1/2 cells were seeded in P6 plates for 24 hours. The following day the medium was changed for a medium with 250 µl of the conditioned medium (static control or fluid flow) and 750 µl of its corresponding culture medium. MC3T3-E1 and C3H/10T1/2 cells were used as control of the experiment and incubated with 250 µL of MEM alpha without phenol red (Gibco) supplemented with 0.5 % of CS, 0.5 % of FBS, 1 % of penicillin-streptomycin, and 750 µl of its corresponding culture medium. After 24 hours, they were incubated with cytopainter for 30 minutes and, after incubation, the cells were lifted, counted, and a total of 20 000 cells/cm^2 were seeded on a new P6 well for 30 minutes. Finally, the supernatant was collected and the cells that were not adhered were counted in a Neubauer chamber using the exclusion method with Trypan blue. On the other hand, images of the cells adhered to the well surface were obtained through a PAULA microscope ("Personal automated lab assistant, Leica Microsystems"). The number of cells marked with fluorescence was counted in 3 different, random fields.

REAL-TIME POLYMERASE CHAIN REACTION (RT-PCR)

A collection of 300 000 cells were seeded in each well in 6-well culture plates in the case of MC3T3-E1 preosteoblastic cells, and 450 000 in the case of C3H/10T1/2 mesenchymal cells. After 24 hours of incubation, the cells were washed with PBS and then PBS was replaced by 250 µl of MEM alpha in the controls and 250 µl in the corresponding conditioned medium in the other wells. In addition, each well was added 750 µl of its corresponding medium. After 24 hours of incubation the culture medium was removed, each medium was collected from the wells in 1.5 mL tubes using trizol and stored at -80 °C.

The following day the samples were defrosted, and kept in ice to maintain a low temperature and then the RNA extraction protocol was performed. Reverse transcription to obtain cDNA was performed with the cDNA reverse transcription kit ("High-capacity RNA-to-cDNA Kit", Thermofisher, 4387406) following the instructions. After the cDNA was obtained, PCR was performed in a P384 plate using the "Sybergreen" (TB Green, Condalab RR420A) to study the following genes: RUNX2, alkaline phosphatase (ALP), PPARγ, and osteocalcin. In addition, beta actin (cytoskeletal actin) was used as constitutive gene expression. To that end, an ABI PRISM 7500 thermocycler was used (Applied Biosystems).

STATISTICAL ANALYSIS

Data are expressed as means ± standard error. The distribution of the data was analyzed and since they did not adjust to a normal distribution, the differences among the experimental groups were evaluated by non-parametric variance analysis (Kruskal-Wallis). Determination of the possible differences among the experimental groups was conducted using the Dunn or Mann-Whitney tests. To conduct the statistical analysis the software GraphPad Prism was used. p values < 0.05 were considered statistically significant.

RESULTS

EFFECTS OF THE CONDITIONED MEDIUM OF MECHANICALLY STIMULATED —OR NOT— OSTEOCYTES ON THE PROLIFERATION OF MESENCHYMAL CELLS AND PREOSTEOBLASTS

Proliferation study of mouse MC3T3-E1 preosteoblastic cells and mesenchymal cells (C3H/10T1/2) was conducted with 25 % of conditioned medium of MLO-Y4 mouse osteocytic cells mechanically stimulated (FF) or not (SC) (Fig. 1).

We observed that in both cell lines the osteocyte secretomes show significant effects in proliferation. While the mechanically stimulated (FF) osteocyte secretome promotes greater proliferation, non-stimulated (SC) osteocytes secretome induces less proliferation versus control (Fig. 1 A and C). No differences were observed in cell viability in any of the three experimental conditions in the 4 days analyzed (Fig. 1 B and D).

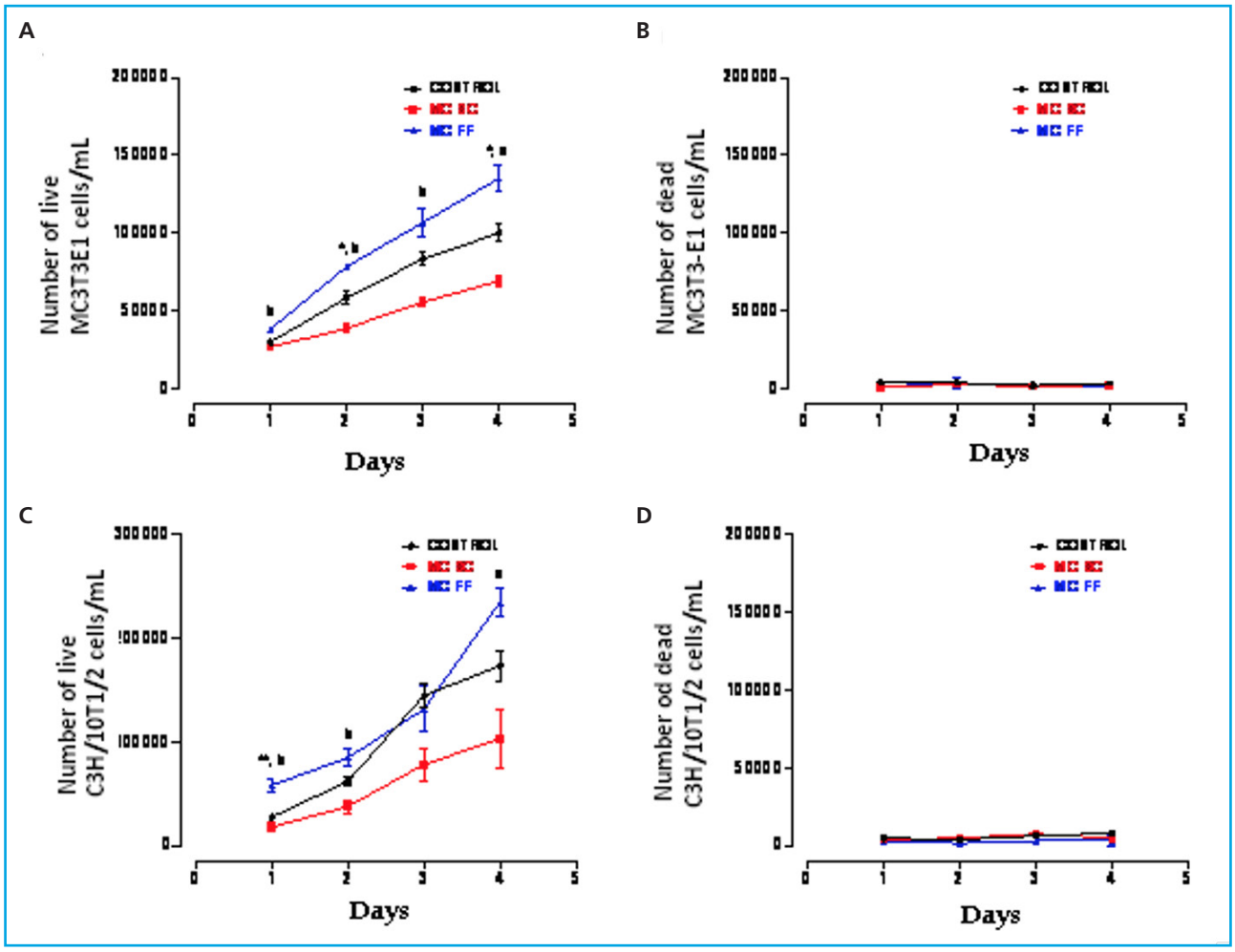

Figure 1. Proliferation and cellular death of MC3T3-E1 preosteoblastic cells (A and B, respectively) and C3H/10T1/2 embryonic mesenchymal cells (C and D, respectively) in the presence or absence of conditioned MLO-Y4 osteocyte media after mechanical stimulation (fluid flow: MC FF) or not (static control: MC SC). The controls represent cells without stimulation of osteocyte conditioned media. The values are the mean ± standard error of the 3 experiments conducted in triplicate. *$p < 0.05$ vs. control; **$p < 0.01$ vs. control; [a]$p < 0.05$ vs. MC SC; [b]$p < 0.01$ vs. MC SC.

EFFECTS OF THE CONDITIONED MEDIA OF MECHANICALLY STIMULATED —OR NOT— OSTEOCYTES ON ADHESION OF MESENCHYMAL CELLS AND PREOSTEOBLASTS

Afterwards, a mouse MC3T3-E1 preosteoblastic cell and mesenchymal cell (C3H/10T1/2) adhesion study was conducted in the presence of secretome of osteocytic MLO-Y4 mouse cells after stimulation (FF) or lack (SC) of mechanical stimulus by fluid passage.

No significant differences were seen in the adhesion of MC3T3-E1 cells in the different experimental conditions (Fig. 2). Regarding the number of unattached cells, we observed that stimulation with conditioned media (FF and SC) hardly decreased adhesion compared to control conditions (Fig. 2).

However, we did observe a clear difference among different experimental conditions in C3H/10T1/2 cell adhesion. The medium conditioned by mechanically stimulated osteocytes increased adhesion of this cell line (Fig. 3).

ANALYSIS OF GENE EXPRESSION IN MESENCHYMAL AND PREOSTEOBLASTIC CELLS TREATED WITH CONDITIONED MEDIA OF OSTEOCYTES WHETHER STIMULATED MECHANICALLY OR NOT

We conducted a study of differentiation markers and bone formation (Runx2, osteocalcin and alkaline phosphatase) and adipogenic differentiation (PPAR$^{\gamma}$)

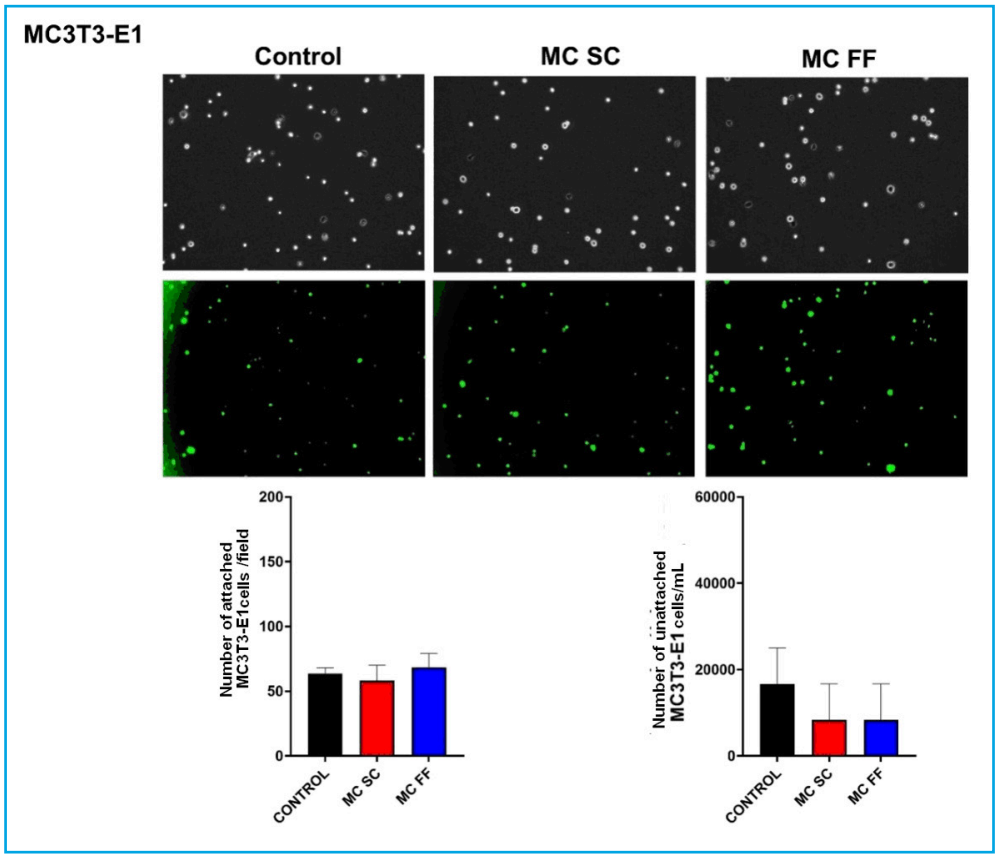

Figure 2. Adhesion of MC3T3-E1 preosteoblastic cells in the presence or absence of conditioned MLO-Y4 osteocyte media after mechanical stimulation (fluid flow: MC FF) or not (static control: MC SC). The controls represent cells without stimulation of osteocyte conditioned media. The values are the mean ± standard error of 3 experiments conducted in triplicate. Representative images are shown after being obtained through bright field microscopy (upper panel) or epifluorescence microscopy (lower panel). Results are expressed as the number of attached cells/field (lower left) and unattached cells/mL (lower right). The values are the mean ± standard error of 3 experiments conducted in triplicate.

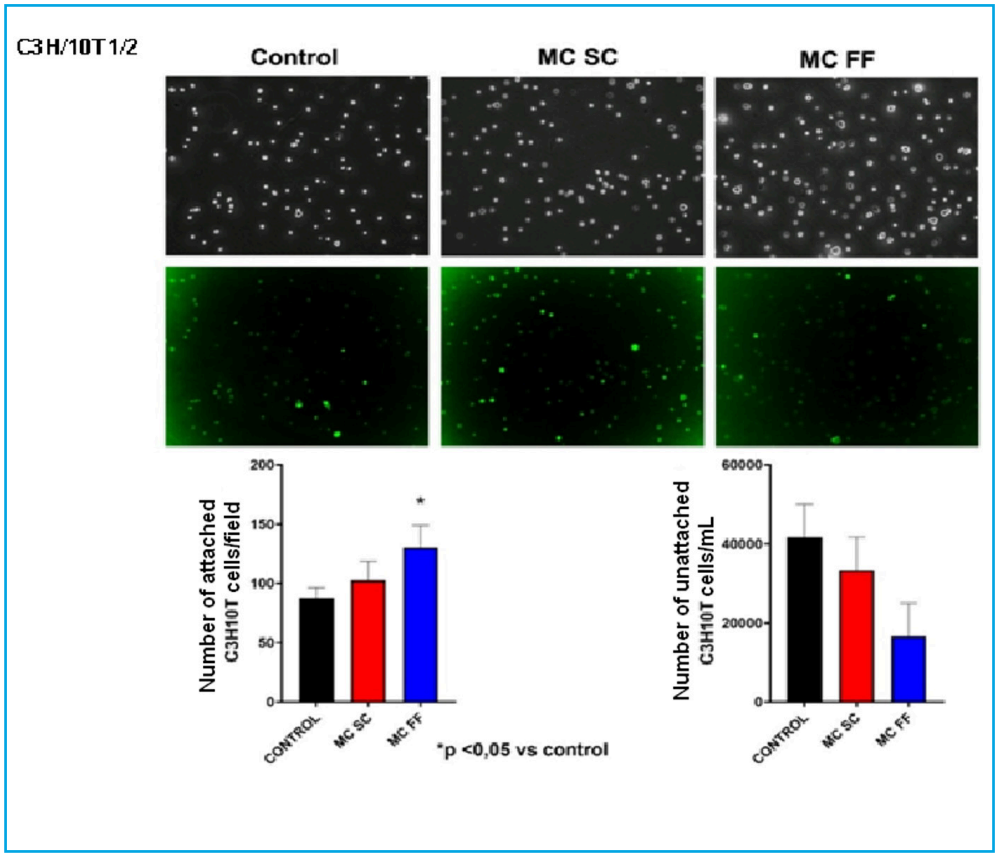

Figure 3. Adhesion of C3H/10T1/2 embryonic mesenchymal cells in the presence or absence of conditioned MLO-Y4 osteocyte media after mechanical stimulation (fluid flow: MC FF) or not (static control: MC SC). The controls represent cells without stimulation of osteocyte conditioned media. The values are the mean ± standard error of 3 experiments conducted in triplicate. Representative images are shown after being obtained through bright field microscopy (upper panel) or epifluorescence microscopy (lower panel). The results are expressed as the number of attached cells/field (lower left) and unattached cells / mL (lower right). The values are the mean ± standard error of 3 experiments conducted in triplicate. *$p < 0.05$ vs. control.

in mouse MC3T3-E1 preosteoblastic cells and mesenchymal cells (C3H/10T1/2) stimulated with 25 % of conditioned media of mouse MLO-Y4 osteocytic cells in the presence (FF) and absence (SC) of a mechanical stimulus by fluid flow. Figures 4 and 5 show no significant changes on the expression of Runx2, osteocalcin, alkaline phosphatase or any of the two lines studied.

However, the PPARγ expression increased after stimulation with conditioned media of osteocytes SC and FF in MC3T3-E1 preosteoblastic cells (Fig. 4) while in C3H/10T1/2 cells, the PPARγ expression levels remained practically unchanged in all the experimental conditions (Fig. 5).

DISCUSSION

Aging and certain bone diseases such as osteoporosis change bone remodeling and associated loss of bone mass. This is due to the accumulation of apoptotic osteocytes and the recruitment of osteoclast precursors that promote the bone resorption process. This situa-

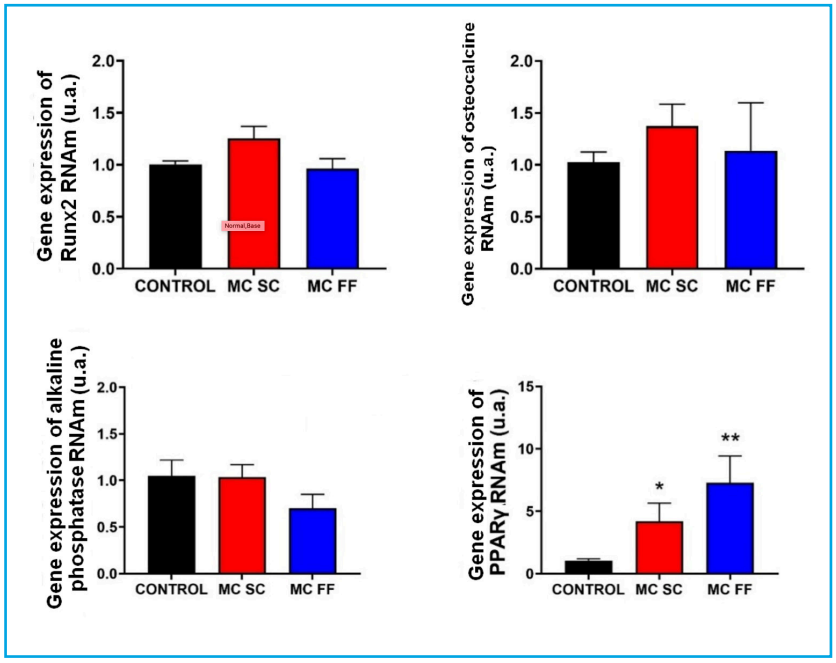

Figure 4. Gene expression analysis of bone differentiation and formation markers (Runx2, osteocalcin, and alkaline phosphatase) and adipogenic differentiation (PPARγ) in MC3T3-E1 preosteoblastic cells in the presence or absence of conditioned MLO-Y4 osteocyte media after mechanical stimulation (fluid flow: MC FF) or not (static control: MC SC). The controls represent cells without stimulation of osteocyte conditioned media. The values are the mean ± standard error of 3 experiments conducted in triplicate. *$p < 0.05$ vs. control; **$p < 0.01$ vs. control.

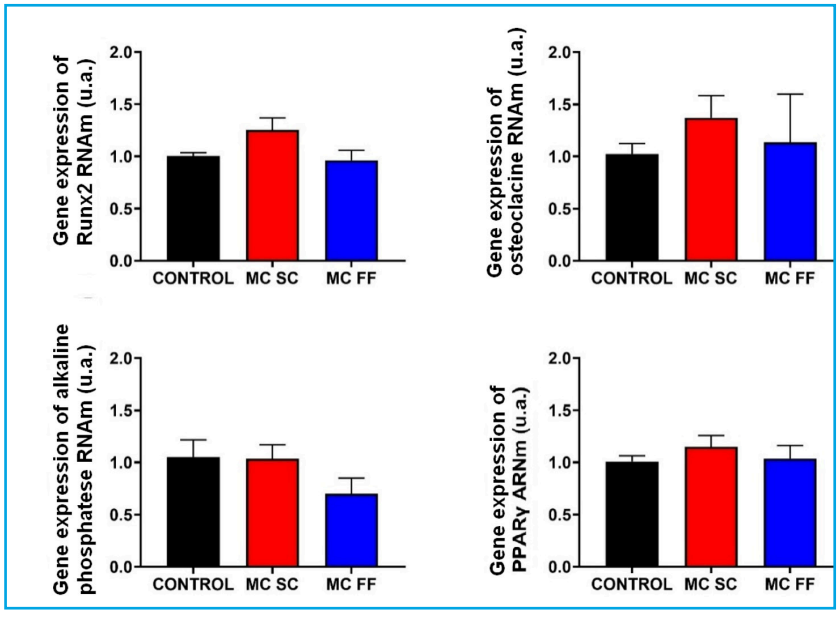

Figure 5. Gene expression analysis of bone differentiation and formation markers (Runx2, osteocalcin, and alkaline phosphatase) and adipogenic differentiation (PPARγ) in C3H/10T1/2 preosteoblastic cells in the presence or absence of conditioned MLO-Y4 osteocyte media after mechanical stimulation (fluid flow: MC FF) or not (static control: MC SC). The controls represent cells without stimulus of osteocyte conditioned media. The values are the mean ± standard error of 3 experiments conducted in triplicate.

tion can be prevented through mechanical stimulation since it is applied naturally on osteocytes when we're doing exercise (8).

Former studies have already demonstrated that the conditioned medium of mechanically stimulated osteocytes can recruit osteoprogenitors (mesenchymal cells and osteoblasts), and promote commitment of osteogenic lineage of these cells to replace exhausted osteoblasts, improve bone formation, and strengthen tissues (9). In addition, mechanical stimulation plays an essential role when it comes to modulating certain cell processes. In our results, we found that exposure of MC3T3-E1 preosteoblastic cells and C3H/10T1/2 mesenchymal cells to conditioned media containing the secretome of mechanically stimulated MLO-Y4 osteocytic cells affects their proliferation and adhesion, as well as the gene expression of the markers studied. Some discrepancies in the results obtained between the two cell lines used in this study can be due to the different nature of each cell type. The MC3T3-E1 preosteoblastic cell line is at a greater degree of differentiation and commitment towards an osteoblastic phenotype compared to C3H/10T1/2 cells. The latter, because they are of embryonic origin, are more undifferentiated and possibly because of this and because of their character as embryonic stem cell, can show greater proliferation compared to more differentiated lines, such as MC3T3-E1 (10).

Regarding the differences of control cells with respect to those exposed to conditioned media, the results could indicate that mechanically stimulated *in vivo* osteocytes maintain bone mass levels when inducing, by secretion of molecules, proliferation of mesenchymal cells that can subsequently be differentiated from osteoblasts that will be making up the bone matrix. However, osteocytes that have not been mechanically stimulated show a modified secretome that probably implies a reduced secretion of proliferating factors that act on mesenchymal cells or increase of secretion of proliferation-inhibiting factors. In any of the two situations, the result would entail less proliferation of mesenchymal cells and possibly less osteoblast differentiation to create the bone matrix.

Because they are less differentiated cells C3H/10T1/2 mesenchymal cells could be considered to show less expression of proteins that are often present in more specialized cells. Therefore, it would be possible that, since they are not committed to a specific cellular phenotype, they can be modified more easily by the secretome of mechanically stimulated osteocytes compared to more differentiated cells like MC3T3-E1 that are already committed to the expression of proteins of osteoblastic lineage. However, the more significant effects of gene expression observed in this study after stimulation with osteocyte secretome are associated with an increased PPARγ expression in MC3T3-E1 cells. This change could be associated with more adipogenesis associated with aging, bone mass loss, and regeneration delay (11), the process opposite to osteoblastogenesis (12), and with the other results obtained in this study. However, some studies indicate that, in some stages of differentiation to osteoblasts PPARγ expression can play an important role (13,14). That is why it will be necessary to conduct more experiments to prove more directly the adipogenic and osteogenic potential of osteocyte secretome on the different types of mesenchymal cells used in this article.

Regarding cell adhesion, for more adhesion to occur an increase in the expression of matrix binding proteins like integrins is often necessary (15). It is possible that, due to overexposure of these matrix binding proteins, mesenchymal cells adhere more easily after being stimulated with mechanically stimulated osteocytes secretome. The adhesive capacity of mesenchymal cells is a necessary requirement for regeneration therapy to occur (16) because, since they are substrate-binding dependent cells, they first need to bind to the damaged areas to be able to start proliferation or differentiation processes.

Therefore, based on our own results, we can assume that certain factors of osteocyte secretome favor mesenchymal cell adhesion, and maybe regeneration processes could indirectly be promoted from these cells.

REFERENCES

1. Hadjidakis DJ, Androulakis II. Bone remodeling. Ann N Y Acad Sci 2006;1092:385-96. DOI: 10.1196/annals.1365.035
2. Stewart S, Darwood A, Masouros S, Higgins C, Ramasamy A. Mechanotransduction in osteogenesis. Bone Joint Res 2020;9(1):1-14. DOI: 10.1302/2046-3758.91.BJR-2019-0043.R2
3. Siddiqui JA, Partridge NC. Physiological Bone Remodeling: Systemic Regulation and Growth Factor Involvement. Physiology (Bethesda) 2016;31(3):233-45. DOI: 10.1152/physiol.00061.2014
4. Schaffler MB, Cheung WY, Majeska R, Kennedy O. Osteocytes: master orchestrators of bone. Calcif Tissue Int 2014;94(1):5-24. DOI: 10.1007/s00223-013-9790-y
5. Pierce JL, Begun DL, Westendorf JJ, McGee-Lawrence ME. Defining osteoblast and adipocyte lineages in the bone marrow. Bone 2019;118:2-7. DOI: 10.1016/j.bone.2018.05.019
6. Lin GL, Hankenson KD. Integration of BMP, Wnt, and notch signaling pathways in osteoblast differentiation. J Cell Biochem 2011;112(12):3491-501. DOI: 10.1002/jcb.23287
7. Wu M, Chen G, Li YP. TGF-β and BMP signaling in osteoblast, skeletal development, and bone formation, homeostasis and disease. Bone Res 2016;4:16009. DOI: 10.1038/boneres.2016.9
8. Cadenas Martín M, Tirado I, Martín E, Ardura J, Bravo B, Gortazar AR. Efectos de la estimulación mecánica en la comunicación entre células óseas. Rev Osteopor Metab Miner 2019;11(1):12-8. DOI: 10.4321/S1889-836X2019000100003
9. Brady RT, O'Brien FJ, Hoey DA. Mechanically stimulated bone cells secrete paracrine factors that regulate osteoprogenitor

recruitment, proliferation, and differentiation. Biochem Biophys Res Commun 2015;459(1):118-23. DOI: 10.1016/j bbrc.2015.02.080
10. Ding DC, Shyu WC, Lin SZ. Mesenchymal Stem Cells. Cell Transplant 2011;20(1),5-14. DOI: 10.3727/096368910X
11. Kawai M, Sousa K, MacDougald O, Rosen C. Themanyfacets of PPARγ: novel insights for the skeleton. Am J Physiol Endocrinol Metab 2010;299(1):E3-E9. DOI: 10.1152/ajpendo.00157.2010
12. Lee S, Choi E, Cha MJ, Hwang KC. Cell Adhesion and Long-Term Survival of Transplanted Mesenchymal Stem Cells: A Prerequisite for Cell Therapy. Oxid Med Cell Longev 2015;2015:632902. DOI: 10.1155/2015/632902
13. Jackson SM, Demer LL. Peroxisome proliferator-activated receptor activators modulate the osteoblastic maturation of MC3T3-E1 preosteoblasts. FEBS Lett 2000;471(1):119-24. DOI: 10.1016/s0014-5793(00)01372-7
14. Yasuda E, Tokuda H, Ishisaki A, Hirade K, Kanno Y, Hanai Y, et al. PPAR-gamma ligands up-regulate basic fibroblast growth factor-induced VEGF release through amplifying SAPK/JNK activation in osteoblasts. Biochem Biophys Res Commun 2005;328(1):137-43. DOI: 10.1016/j.bbrc.2004.12.163
15. Moreno-Layseca P, Icha J, Hamidi H, Ivaska J. Integrin trafficking in cells and tissues. Nat Cell Biol 2019;21(2):122-32. DOI: 10.1038/s41556-018-0223-z
16. Chamberlain G, Fox J, Ashton B, Middleton J. Concise Review: Mesenchymal Stem Cells: Their Phenotype, Differentiation Capacity, Immunological Features, and Potential for Homing. Stem Cells 2007;25(11):2739-49. DOI: 10.1634/stemcells.2007-0197

Revista de Osteoporosis y Metabolismo Mineral

Review

Genome-wide association studies (GWAS) *vs* functional validation: the challenge of the post-GWAS era

Núria Martínez-Gil, Juan David Patiño-Salazar, Raquel Rabionet, Daniel Grinberg, Susanna Balcells

Department of Genetics, Microbiology and Statistics. Faculty of Biology. Universitat de Barcelona. CIBERER, IBUB, IRSJD. Barcelona, Spain

Abstract

Over the past few years, efforts have been made to determine the variants and genes that may be important to determine bone mineral density (BMD) that, at the same time, are involved in several bone diseases. To achieve this, the approach that has been the most successful of all has been genome-wide association studies (GWAS). In particular, in research on bone biology over 50 different large GWAS or GWAS metanalyses have been published identifying a total of 500 genetic *loci* associated with different bone parameters such as BMD, bone resistance, and risk of fracture. Although the discovery of associated variants is an essential aspect, the functional validation of such variants is equally important to elucidate their effect, as well as the causal correlation they have with genetic disease. Since it is a much more time consuming and tedious aspect it has become the new challenge of this post-GWAS era. Among the genes that have already been studied several Wnt signaling pathway genes have been included, among them, the *SOST* gene that plays a crucial role both determining the BMD of the population and monogenic diseases with elevated bone mass giving rise to a new therapy against osteoporosis. In this review we'll be collecting the main GWAS associated with bone phenotypes, as well as some functional validations undertaken to analyze the associations found in them.

Keywords: Genome-wide association studies. Functional validation. Bone mineral density. Bone diseases.

Received: 20/07/2022 • Accepted: 22/12/2022

This article has been submitted in full compliance with the commitment made after receiving the 2019 FEIOMM Research GRANT to conduct the Functional Studies Project of gen CYP1A1 variants producing functional changes found in patients with atypical femoral fractures.

Conflict of interest: the authors declare no conflict of interest.

Martínez-Gil N, Patiño-Salazar JD, Rabionet R, Grinberg D, Balcells S. Genome-wide association studies (GWAS) *vs* functional validation: the challenge of the post-GWAS era. Rev Osteoporos Metab Miner 2023;15(1):29-39

DOI: 10.20960/RevOsteoporosMetabMiner.00008

Correspondence:

Susanna Balcells Comas. Department of Genetics, Microbiology and Statistics. Faculty of Biology. Universitat de Barcelona. Avda. Diagonal, 643. 08028 Barcelona, Spain
e-mail: sbalcells@ub.edu

GENOME-WIDE ASSOCIATION STUDIES (GWAS)

Over the past few years, genome-wide association studies (GWAS) have been an essential tool to identify what genes are involved in complex diseases (1). These studies consist of establishing an association between the genetic or allelic frequency of millions of SNP (single nucleotide polymorphisms) type markers distributed across the genome and a particular phenotype or disease (2). This approach is the most complete and impartial tool that exists for the particular of complex diseases. Unlike candidate gene association studies, GWAS are a hypothesis-free approximation hypothesis that allows the discovery of new genes or signaling pathways involved in a given phenotype that, up until now, were completely unknown (3). GWAS has been possible thanks to new advances made in high-throughput genome technology, study design, improved statistical analysis, and the possibility of having large biobanks available (4,5). Due to the large number of simultaneous statistical tests performed and, therefore, the statistical corrections made (that require a threshold *p* value of $5x10^{-8}$ to be considered statistically significant at whole genome level, and the small effect each variant presents in complex diseases, extremely large cohorts are required. This has been achieved through metanalyses of the GWAS where different studies have come together to increase the size of the sample (6,7).

Although with the evident success reported, GWAS have 3 main limitations. First, the genetic variants used to validate the association with the particular phenotype are SNP markers (tagSNPs) that are homogeneously distributed across the whole genome with a minor allele frequency (MAF) ≥ 5 % in the population. Therefore, rare variants with possible strong effects in the phenotype are not included in these studies. An attempt has been made to solve this limitation by including variants of less frequency in genotype chips, whole exome/genome sequencing, WES/WGS) and/or using the phenotypic extremes of the cohorts. Second, the success of GWAS largely depends on the size of the sample. Therefore, as commented above, the most widely used strategy today is to establish large consortia including different cohorts from across the world. Therefore, super-cohorts of greater statistical power —but genetically heterogeneous— are obtained in such a way that variants of a specific population are very difficult to find. Third, GWAS report the most statistically relevant SNP called lead SNP. Although this SNP can be the one causing this association, other variants that are in linkage disequilibrium with respect to the lead SNP variant can be responsible too. If the SNP associated is found in a codifying region and involves a change of amino acid, chances are that the SNP will be causal. However, truth is that most lead SNPs can be found in non-codifying regions (96 %) both intronic (41 %) and intergenic (54 %), which complicates the demonstration of their causal roles. Due to their non-coding nature, conducting functional studies of these lead SNPs is truly challenging (8-10). Therefore, these functional studies are still scarce to this date, and establishing the functional basis of the associations found in such analyses is still to be elucidated in this post-GWAS era.

To conduct functionality studies, interdisciplinary approaches are needed including *in silico* analyses (computational approaches) (11,12) —like pathogenicity prediction tools—, *in vitro* studies including, among other, studies of the reporter gene assays (eg, luciferase) (13) and *in vivo* studies of animal models like the zebra fish or mice (14,15).

This review summarizes the main GWAS published to this date using skeletal phenotypes, followed by *in vitro* and *in vivo* studies generated from the first large GWAS metanalysis (16) ever conducted on bone mineral density (BMD) and risks of fracture.

GWAS AND BONES

To conduct GWAS of bone diseases such as osteoporosis, parameters like BMD, and the geometry and microarchitecture of the bone can be taken into consideration. Among these properties, the most widely used and the one that best predicts osteoporotic fracture is BMD that is a quantitative trait measured in a continuous scale using methods like dual-energy X-ray absorptiometry (DXA). It is estimated that BMD is a trait with an approximate heritability between 50 % and 80 %. Similarly, the geometry of the bone shows heritability rates between 30 % and 70 % while bone microarchitecture determined by high-resolution peripheral quantitative computed tomography scan (HR-pQCT) shows heritability rates between 20 % and 80 % (17).

Up until now, over 50 large GWAS have been conducted using bone parameters together with a plethora of GWAS in smaller and more homogenous cohorts. With this over 500 associated *loci* have been identified. Although the percentage of variance explained through GWAS has increased substantially over the past few years thanks to the use of larger cohorts, all these *loci* only explain a small percentage (20 %) of genetic contribution to BMD (18,19). This has created a gap between the variability explained by genetic factors and BMD heritability probably due to overestimating heritability or the fact that other genetic factors like copy number variants (CNV) or epigenetics are not being taken into consideration (20).

All in all, GWAS have yielded significant findings like the association between the *SOST* and *LRP5* genes —that had already been involved in monogenic skeletal disorders— and some skeletal phenotypes or the identification of new genes whose involvement in bone phenotypes was previously unknown (21). Table I

shows some of the most relevant GWAS associated with BMD, most of which have been reported in the GWAS catalog (http:\\ebi.ac.uk/gwas). To narrow it down, only studies with cohorts > 10 000 individuals have been considered.

Many of the GWAS displayed on table I correspond to studies in which large metanalyses have been conducted leaving as a result hundreds of variants in different *loci* associated with skeletal phenotypes. However, most of these studies lack functional approaches.

FUNCTIONAL STUDIES IN THE POST-GWAS ERA

Despite the huge amount of association studies conducted to this date, functional studies have not developed at the same pace. Therefore, only a small fraction (164; 15 %) of the 1051 manuscripts that have cited the first large GWAS metanalysis on bone density (16) included functional studies whether *in vitro* or *in vivo.*

An example of successful functional studies is the characterization of the regulation of the *SOST* gene. This gene codes the sclerostin protein, a canonical Wnt signaling pathway inhibitor (49-51) associated with multiple bone parameters in different association studies across several populations (17,28,33,38,40,43,52,53) (Fig. 1A). Its inhibitory function on bone formation has been widely studied in *in vivo* and *in vitro* models. Currently, antisclerostin antibodies are used to treat bone diseases like osteoporosis or osteogenesis imperfecta (54-59). Therefore, the regulatory factors of the expression of the *SOST* gene are included among the new candidates as a target for the development of new therapies. In humans, *SOST* gene variants have been associated with conditions characterized by an excessive bone formation: sclerosteosis, craniodiaphyseal dysplasia, and the phenotypic trait of high bone mass (60) (Fig. 1B). To these diseases we may add Van Buchem disease. It is due to the deletion of the enhancer element ECR5 of *SOST* situated at the 52 kb region downstream of the gene that is necessary for the proper expression of the *SOST* gene (61) (Fig. 1A). Actually, the transcription of the *SOST* gene is finely regulated by many different signals both through direct regulation on the promoter of the *SOST* gene and through the distal ECR5 regulatory region (62,63) whose physical interaction has been demonstrated in a study recently conducted by our group on bone cells (64) (Fig. 1A). The MEF2C transcription factor is the best described *SOST* regulator in relation to its expression in osteocytes (63,65). The importance of MEF2C in the enhancer effect of ECR5 has been confirmed in the knock-out mouse model of *Mef2c* in osteoblasts/osteocytes that has a high bone mass and low levels of sclerostin (66). Precisely, *MEF2C* is yet another of the most repeated signals in GWAS with bone parameters (16,23,36,37,67-70). Together with MEF2C, HDAC5 has also been described as a negative regulator of the expression of the SOST gene that exerts its function by blocking the association of MEF2C and ECR5 during the differentiation of immature osteocytes (Fig. 1C). Consistent with this, the *HDAC4/5* knock-out mouse model displays low BMD, and high expression of the SOST gene (71-73). Once again, *HDAC4/5* is found among the most repeated *loci* in association studies with bone parameters (18,23,34,39,74) (Fig. 1B).

Another example of how important it is to conduct functional studies of associated regions is the *DKK1 locus.* This is another canonical Wnt signaling pathway inhibitor that plays a crucial role in the morphogenesis of the head (75,76), and bone development (77,78). Currently, no *DKK1* variant has been described causing bone diseases in the HGMD database. Despite of this, our group identified 2 different missense variants in patients with the high BMD phenotype who show a functional loss of their inhibitory ability (13,79). On the other hand, one of these variants has also been found in patients with totally opposed phenotypes like osteoporosis or anal malformations (80,81). Also, we should mention that no GWAS has ever found SNPs in *DKK1* associated with BMD or other bone parameters. However, an association with BMD has been demonstrated in a set of SNPs grouped in a region 350 kb downstream of *DKK1* and 92 kb upstream of *MBL2* (16,18,19,29,33,34,36,37,39,74) (Fig. 2). To distinguish which one of these 2 genes was responsible for this association, a study from our group (13) conducted a 4C chromatin conformation capture using the GWAS signal-rich region as a bait in 3 bone cellular types. This confirmed the physical interaction between this region and the *DKK1* promoter ruling out any interaction with the *MBL2* gene (Fig. 2; lower panel). It is precisely in this region where the *LNCAROD* gene is found, which specifies a DKK1 activator long noncoding (lncRNA), a possible culprit of the association found in the GWAS (82).

One of the most consistent *loci* across different GWAS on BMD is the genomic region situated in 7q31.31 including the *WNT16* gene. This is a very complex *loci,* also including, apart from the *WNT1* gene, the neighboring genes *ING3, FAM3C,* and *CPED1.* The role of the *WNT16* gene determining BMD has been clearly established in functional studies of knock-out mouse models or osteoblast-specific conditional knock-out mice (6,83,84) that, largely, show spontaneous fractures due to low BMD plus reduced cortical thickness and bone resistance. However, evidence has been found on the importance of 3 other neighboring genes in bone metabolism. In the case of the protein coding gene *ING3* (Inhibitor of Growth Family Member 3) —part of the Nucleosome Acetyltransferase of H4 histone acetylation (NuA4 HAT) complex involved in chromatin regulation— it has been found abundantly expressed in bone tissue (85).

Table I. GWAS on bone and genes found with variants associated with skeletal phenotypes

Study	Ancestry	Trait	Sample size	Most relevant *loci*/genes	Brand-new *loci*/genes
Styrkarsdottir *et al.*, 2009 (22)	European	BMD-LS, BMD-FN, OF	15 375	*MARK3, SOST, SP7 (osterix)*	4/9
Rivadeneira *et al.*, 2009 (23)	European	BMD-LS, BMD-FN	19 195	*WLS, CTNNB1, MEPE, STARD3NL, FLJ42280, DCDC5, SOX6, FOXL1, HDAC5, CRHR1, MEF2C*	13/20
Guo *et al.*, 2010 (24)		BMD-Th	11 568	*ALDH7A1*	1/1
Kung *et al.*, 2010 (25)	Asian	BMD-LS, BMD-FN, OF	18 898	*JAG1*	1/1
Hsu *et al.*, 2010 (26)	European	BMD-LS, BMD-FN, FN-AA, WNS, LFN	11 290	*RAP1A, TBC1D8, OSBPL1A*	3/4
Estrada *et al.*, 2012 (16)	European and Asian	BMD-LS, BMD-FN, OF	83 894	*CDKAL/SOX4, CPED1, WNT16, MBL2/DKK1, AXIN1, RPS6KA5, ERC1/WNT5B, FAM210A, FAM9B/KAL1, SOX9, KLHDC5/PTHLH, IDUA, NTAN1, SFRP4, SUPT3H/RUNX2*	32/56
Styrkarsdottir *et al.*, 2013 (27)	European	BMD-LS, BMD-WB, BMD-h, OF	97 315	*LGR4*	1/2
Zhang *et al.*, 2014 (28)	European, Asian, and African American	BMD-LS, BMD-FN, BMD-Th	27 061	*SMOC1, CLDN14*	2/15
Moayyeri *et al.*, 2014 (29)	European, Asian, and North American	BUA, SS, BMD-H	59 242	*TMEM135*	1/7
Zheng *et al.*, 2015 (30)	European	BMD-LS, BMD-FN, BMD-F, OF	561 489	*EN1*	1/36
Styrkarsdottir *et al.*, 2016 (31)	European and Asian	BMD-LS, BMD-h, OF	30 191	*PTCH1*	1/14
Nielson *et al.*, 2016 (32)	European, and North American	BMD-LS, CVF, RVF	42 869	*SLC1A3/RANBP3L*	1/5
Mullin *et al.*, 2017 (33)	European	BUA, SS, OF	16 627	*PPP1R3B, LOC387810, SEPT5/TBX1*	3/8
Kemp *et al.*, 2017 (34)	European	eBMD-H, OF	142 487	*ARID1A, PKN2, TBX15, NGEF, SUSD5, ERC2, BMP2, PLXDC2, BMP5, MEOX2, CREB5, AQP1, CADM1, EMP1, NFATC1, TMEM92, GPC6, BMP4, SMAD3, BMPR2, AXIN2*	153/203
den Hollander *et al.*, 2017 (35)	European, and North American	BSGH, OA	12 784	*MGP, CCDC91*	2/5
Medina-Gomez *et al.*, 2018 (36)	European, African American, and Australian	BMD-WB	66 628	*SLC8A1, PLCL1, SMAD9, ADAMTS5, TOM1L2, TCF7L1, APC, DUSP5, CD44, CCND1, CYP19A1, MAFB, RUNX1, RAI1, ZSCAN25, GRB10, DRG2, ETS2, PSMD13, CSF1*	36/80
Pei *et al.*, 2018 (37)	European, Asian, African American, and Hispanic	BMD-LS, BMD-FN	40 449	*MACROD2, OSBPL2*	2/9
Alonso *et al.*, 2018 (38)	European, and Australian	CVF	10 683	*2q13*	1/1
S. K. Kim 2018 (39)	Europea	DMOe-T, FO	394 929	*RP1L1, PRSS55, MAPT, GPATCH1, SMG6, WNT1, WNT5B*	613/899

(Continues on next page)

Table I (Cont.). GWAS on bone and genes found with variants associated with skeletal phenotypes

Study	Ancestry	Trait	Sample size	Most relevant *loci*/genes	Brand-new *loci*/genes
Trajanoska *et al.*, 2018 (19)	European, North American, Asian, and Australian	OF	562 258	*GRB10/COBL, ETS2, RSPO3*	4/15
Baird *et al.*, 2019 (40)	European, North American, and Australian	DXA-h	15 934	*ASTN2, PTHLH, NKX3-2, FGFR4, GSC/DICER1, HHIP*	6/8
Hsu *et al.*, 2019 (41)	European, North American, and Asian	LFN, AA, WNS, MSFN	18 719	*IRX1/ADAMTS167*	1/4
Morris *et al.*, 2019 (18)	European	eBMD-H, OF	426 824	*DAAM2, WNT7B, WNT2B, COL11A1, SERPINC1, PRKCE, HDAC4, HOXD11, BCL11A, SOX5, TGFBR3, MMP16, EPHA4, MSH6, SEPT11, LRRC1, ADH1B, CTPS1, DNMT3A, MEIS1*	301/518
Pei *et al.*, 2019 (42)	European, North American, and Australian	BMD-H, BMD-WB	209 115	*FBN2, DEF6, TNFRSF19, NFE2L1, SCMH1*	18/56
Styrkarsdottir *et al.*, 2019 (43)	European and Asian	BMD-h, BMD-LS-BA, OF	28 954	*GDF5, ADAMTSL3, BCKDHB, CHRDL2, DYM, CTDSP2*	6/13
Zheng *et al.*, 2019 (44)	European, North American, and Australian	BMD-FN, eBMD-HU	10 584	*B4GLANT3, GALNT1*	2/3
Feng *et al.*, 2020 (45)	European, North American, African American, Asian, and Hispanic	BMD-h, TLM, eBMD-H	11 335	*MC4R*	1/2
Zhang *et al.*, 2020 (46)	European, North American, African American, Asian, and Hispanic	BMD-FN, BLMAL	12 445	*FTO, PPP1CB, TRMT61B, LSAMP, FAM189A2, LOC101928063*	6/26
Surakka *et al.*, 2020 (47)	European	BMD-F	19 705		0/10
Greenbaum *et al.*, 2022 (48)	European,	DMO-CF, DMO-CL	49 487	*IGF2, ZNF423, SIPA1, PED4D, PIGN, TRAF3IP2, NFIB, LYSMD4, MAML2*	9/30

The study is represented by the first author and year. The genes are the study most relevant ones due to their association with skeletal phenotypes and their new finding. AA, axis angle; BLMAL, body lean mass of arms and legs; BMD, bone mineral density; BS, bone size; BSGH, bilateral semi-quantitative grading of the hand; BUA, broadband ultrasound attenuation; CVF, clinically confirmed vertebral fracture; DXA-h, X-ray absorptiometry of the shape of the hip; eBMD, estimated bone mineral density; F, forearm; FN, femoral neck; H, heel; h, hip; HU, heel ultrasound; LFN, length of the femoral neck; LS-BA, lumbar spine-bone area; LS, lumbar spine; MSFN, modular section of femoral neck; OA, osteoarthritis; OF, osteoporotic fracture; RVF, radiographically confirmed vertebral fracture; SS, speed of sound; Th, total hip; TLM, trunk lean mass; WB, whole body; WNS, width of the neck narrow section.

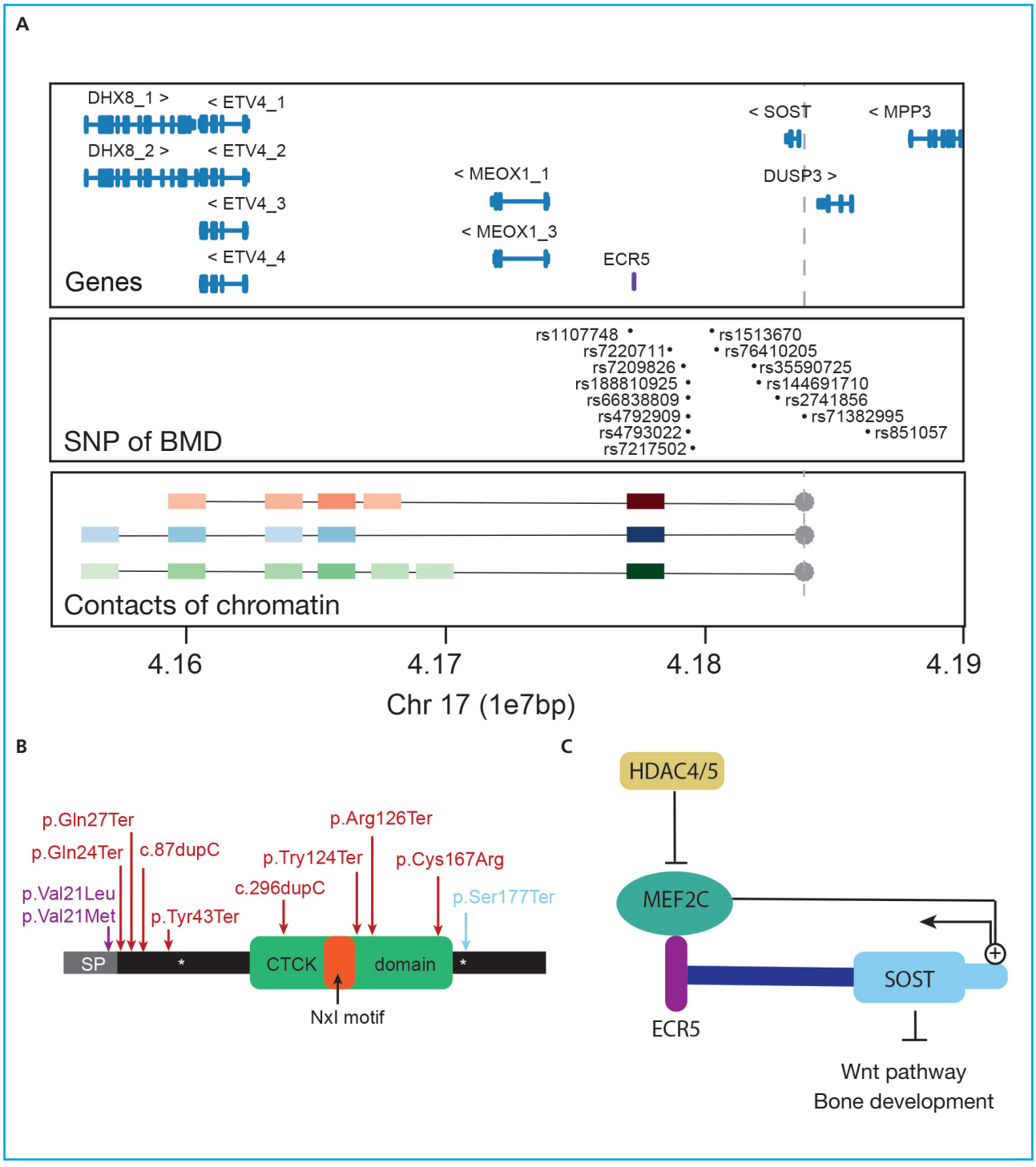

Figure 1. The *SOST* gene. A. Upper panel: *Locus* containing the *SOST* gene and its neighboring genes (GRC37/hg19). In purple, the ECR5 regulatory region. Main panel: SNPs associated with different bone parameters across different GWAS from the GWAS catalogue (https://www.ebi.ac.uk/gwas7). Lower panel: Main results of the 4C clinical trial conducted by Martínez-Gil et al. back in 2021 showing the main interactions of the SOST promoter (used as a bait and indicated with a dot and gray discontinuous). Colored squares show the interactions with color intensity proportional to the intensity of the interaction. Red, blue, and green squares show interactions with mesenchymal stem cells, hFOB cells, and SAOS2 cells, respectively. The units of the genomic scale used (1e7pb) correspond to 10 mega bases ($1x10^7$ base pairs). B. Schematic representation showing of sclerostin protein showing its functional domains and variants responsible for human skeletal conditions. Purple, red, and blue colors show the variants associated with craniodiaphyseal dysplasia, sclerosteosis, and the HBM phenotype variant. CTCK, C/terminal cysteine knot-like. C. Scheme of some of the positive and negative regulators of the expression of the *SOST* gene.

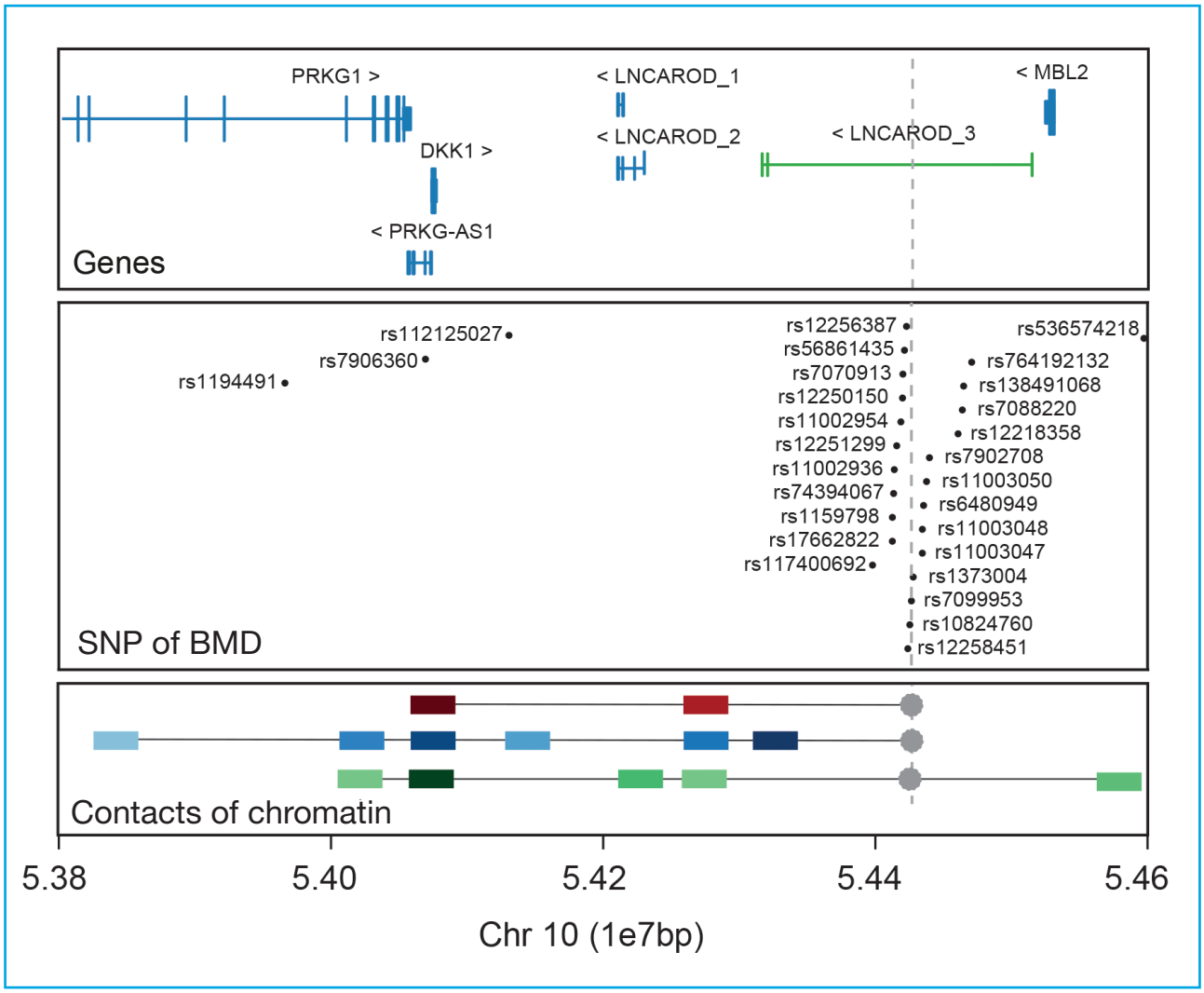

Figure 2. DKK1. Upper panel: *locus* containing the *DKK1* gene and its neighboring genes (GRC37/hg19). In green, the lncRNA *LNCAROD* of GENCODE v32.2 (GRC38/hg18). Main panel: SNPs associated with different bone parameters across different GWAS taken from the GWAS catalogue (https://www.ebi.ac.uk/gwas7). Lower panel: Main results from the 4C clinical trial conducted by Martínez-Gil et al. in 2020 showing the main interactions with the SNP-rich region associated with BMD (used as a bait and indicated with a dot and gray discontinuous line). Colored squares show interactions with color intensity proportional to the intensity of the interaction. Red, blue, and green squares show interactions with mesenchymal stem cells, hFOB cells, and SAOS2 cells, respectively. The units of the genome scale used (1e7pb) correspond to10 mega bases ($1x10^7$ base pairs).

In addition, functional studies of an *in vitro* cellular model of mesenchymal cells knocked-out for *ING3* show osteoblastogenesis damage and stimulation of adipogenic differentiation (86). Regarding the *CPED1* gene (Cadherin Like And PC-Esterase Domain Containing 1), no specific function of this gene has been found in humans or mice. However, in mice, functional studies show that the *Cped1* gene is uniformly expressed in a variety of tissues including bone. Also, different isoforms have been described due to alternative splicing, as well as 3 promoter regions active during osteogenic differentiation (87). To better define its possible role in bone homeostasis, additional functional studies would be needed in *in vitro* cellular or animal models. *FAM3C* (family of sequence similarity 3c) is a cytokine-like growth factor expressed in multiple tissues (88) that plays a very important role in epithelial-mesenchymal transition, and cancer metastasis (89). Its association with bone metabolism has been confirmed with the knock-out mouse model that shows bone structure alterations (88).

Several functional studies have been conducted on the expression regulation of different genes at that region. For example, our group has conducted eQTL studies (expression Quantitative Trait Locus) with primary osteoblasts that show that SNPs located inside the *WNT16* gene regulate the levels of expression of *FAM3C* of those cells (90). Also, in cells of osteoblastic lineage we have seen a physical interaction among different gene enhancers located inside the *CPED1* gene, and the promoter of the *WNT16* gene (91). All this shows the existence of a complex relation among these 4 genes, and suggests the possibility that they are working together. All in all, additional functional studies should be conducted to elucidate the role played by each of these genes, as well as all their possible interactions.

The aforementioned studies reveal the importance of functional studies based on the findings brought by analyzing GWAS. Challenge, now, is in the post-GWAS era. If we keep finding correlations between different variants in GWAS and functional aspects of these variants —*in silico, in vitro* or *in vivo*— we may end up finding new approaches and, therefore, new insights and therapeutic options for associated conditions and disorders.

REFERENCES

1. Lichou F, Gosia T. Functional studies of GWAS variants are gaining momentum. Nat Commun 2020;11(1):6283. DOI: 10.1038/s41467-020-20188-y
2. Manolio TA. Genomewide association studies and assessment of the risk of disease. N Engl J Med 2010;363(2):166-76. DOI: 10.1056/NEJMra0905980
3. Cannon ME, Karen LM. Deciphering the emerging complexities of molecular mechanisms at GWAS loci. Am J Hum Genet 2018;103(5):637-53. DOI: 10.1016/j.ajhg.2018.10.001
4. Visscher PV, Wray N, Zhang Q, Sklar P, McCarthy M, Brown M, et al. 10 Years of GWAS discovery: biology, function, and translation. Am J Hum Genet 2017;101(1):5-22. DOI: 10.1016/j.ajhg.2017.06.005
5. Buniello A, MacArthur J, Cerezo M, Harris L, Hayhurst J, Malangone C, et al. The NHGRI-EBI GWAS Catalog of published genome-wide association studies, targeted arrays and summary statistics 2019. Nucleic Acids Res 2019;47(D1):D1005-12. DOI: 10.1093/nar/gky1120
6. Medina-Gomez C, Kemp J, Estrada K, Eriksson J, Liu J, Reppe S, et al. Meta-analysis of genome-wide scans for total body BMD in children and adults reveals allelic heterogeneity and age-specific effects at the WNT16 locus. PLoS Genet 2012;8(7):e1002718. DOI: 10.1371/journal.pgen.1002718
7. Loic Y, Sidorenko J, Kemper K, Zheng Z, Wood A, Weedon M, et al. Meta-analysis of genome-wide association studies for height and body mass index in ~700000 individuals of European ancestry. Hum Mol Genet 2018;27(20):3641-9. DOI: 10.1093/hmg/ddy271
8. Tam V, Patel N, Turcotte M, Bossé Y, Paré G, Meyre D. Benefits and limitations of genome-wide association studies. Nat Rev Genet 2019;20(8):467-84. DOI: 10.1038/s41576-019-0127-1
9. Hirschhorn JN. Genomewide association studies — illuminating biologic pathways. N Engl J Med 2009;360(17):1699-701. DOI: 10.1056/NEJMp0808934
10. Klein RJ, Xing X, Mukherjee S, Willis J, Hayes J. Successes of genome-wide association studies. Cell 2010;142(3):350-1.
11. Schaid DJ, Chen W, Larson NB. From Genome-wide associations to candidate causal variants by statistical fine-mapping. Nat Rev Genet 2018;19(8):491-504.
12. Broekema RV, Bakker OB, Jonkers IH. A practical view of fine-mapping and gene prioritization in the post-genome-wide association era. Open Biol 2020;10(1):190221. DOI: 10.1098/rsob.190221
13. Martínez-Gil N, Roca-Ayats N, Atalay N, Pineda-Moncusí M, Garcia-Giralt N, Van Hul W, et al. Functional assessment of coding and regulatory variants from the DKK1 locus. JBMR plus 2020;4(12):e10423. DOI: 10.1002/jbm4.10423
14. Schartl M. Beyond the zebrafish: diverse fish species for modeling human disease. Dis Model Mech 2014;7(2):181-92. DOI: 10.1242/dmm.012245
15. Rao S, Yao Y, Bauer DE. Editing GWAS: experimental approaches to dissect and exploit disease-associated genetic variation. Genome Med 2021;13(1):41. DOI: 10.1186/s13073-021-00857-3
16. Estrada K, Styrkarsdottir U, Evangelou E, Hsu YH, Duncan EL, Ntzani EE, et al. Genome-wide meta-analysis identifies 56 bone mineral density loci and reveals 14 loci associated with risk of fracture. Nat Genet 2012;44(5):491-501. DOI: 10.1038/ng.2249
17. Trajanoska K, Rivadeneira F. The genetic architecture of osteoporosis and fracture risk. Bone 2019;126:2-10.
18. Morris JA, Kemp JA, Youlten SE, Laurent L, Logan JG, Chai RC, et al. An atlas of genetic influences on osteoporosis in humans and mice. Nat Genet 2019;51(2):258-66.
19. Trajanoska K, Morris JA, Oei L, Zheng H-F, Evans DM, Kiel DP, et al. Assessment of the genetic and clinical determinants of fracture risk: genome wide association and mendelian randomisation study. BMJ 2018;362:k3225. DOI: 10.1016/j.bone.2019.04.005
20. García-Ibarbia C, Delgado-Calle J, Casafont I, Velasco J, Arozamena J, Pérez-Núñez M, et al. Contribution of genetic and epigenetic mechanisms to Wnt pathway activity in prevalent skeletal disorders. Gene 2013;532(2):165-72. DOI: 10.1016/j.gene.2013.09.080
21. Ohkawara B, Cabrera-Serrano M, Nakata T, Milone M, Asai N, Ito K, et al. LRP4 third β-propeller domain mutations cause novel congenital myasthenia by compromising agrin-mediated MuSK signaling in a position-specific manner. Hum Mol Genet 2014;23(7):1856-68. DOI: 10.1093/hmg/ddt578
22. Styrkarsdottir U, Halldorsson BV, Gretarsdottir S, Gudbjartsson DF, Walters GB, Ingvarsson T, et al. New sequence variants associated with bone mineral density. Nat Genet 2009;41(1):15-7. DOI: 10.1038/ng.284
23. Rivadeneira F, Styrkársdottir U, Estrada K, Halldórsson BV, Hsu Y-H, Richards JB, et al. Twenty bone-mineral-density loci identified by large-scale meta-analysis of genome-wide association studies. Nat Genet 2009;41(11):1199-206. DOI: 10.1038/ng.446
24. Guo Y, Tan L-J, Lei S-F, Yang T-L, Chen X-D, Zhang F, et al. Genome-wide association study identifies ALDH7A1 as a novel susceptibility

gene for osteoporosis. PLoS Genet 2010;6(1):e1000806. DOI: 10.1371/journal.pgen.1000806
25. Kung AW, Xiao SM, Cherny S, Li GH, Gao Y, Tso G, et al. Association of JAG1 with bone mineral density and osteoporotic fractures: a genome-wide association study and follow-up replication studies. Am J Hum Genet 2010;86(2):229-39. DOI: 10.1016/j.ajhg.2009.12.014
26. Hsu YH, Zillikens MC, Wilson SG, Farber CR, Demissie S, Soranzo N, et al. An integration of genome-wide association study and gene expression profiling to prioritize the discovery of novel susceptibility loci for osteoporosis-related traits. PLoS Genet 2010;6(6):e1000977. DOI: 10.1371/journal.pgen.1000977
27. Styrkarsdottir U, Thorleifsson G, Sulem P, Gudbjartsson DF, Sigurdsson A, Aslaug J, et al. Nonsense mutation in the LGR4 gene is associated with several human diseases and other traits. Nature 2013;497(7450):517-20. DOI: 10.1038/nature12124
28. Zhang L, Choi HJ, Estrada K, Leo PJ, Li J, Pei Y-F, et al. Multistage genome-wide association meta-analyses identified two new loci for bone mineral density. Hum Mol Genet 2014;23(7):1923-33. DOI: 10.1093/hmg/ddt575
29. Moayyeri A, Hsu Y-H, Karasik D, Estrada K, Xiao S-M, Nielson C, et al. Genetic determinants of heel bone properties: genome-wide association meta-analysis and replication in the GEFOS/GENOMOS consortium. Hum Mol Genet 2014;23(11):3054-68. DOI: 10.1093/hmg/ddt675
30. Zheng H-F, Forgetta V, Hsu Y-H, Estrada K, Rosello-Diez A, Leo PJ, et al. Whole-genome sequencing identifies EN1 as a determinant of bone density and fracture. Nature 2015;526(7571):112-7. DOI: 10.1038/nature14878
31. Styrkarsdottir U, Thorleifsson G, Gudjonsson SA, Sigurdsson A, Center JR, Hun Lee S, et al. Sequence variants in the PTCH1 gene associate with spine bone mineral density and osteoporotic fractures. Nat Commun 2016;7:10129. DOI: 10.1038/ncomms10129
32. Nielson C, Liu C-T, Smith AV, Ackert-Bicknell C, Reppe S, Jakobsdottir J, et al. Novel genetic variants associated with increased vertebral volumetric BMD, reduced vertebral fracture risk, and increased expression of SLC1A3 and EPHB2. J Bone Miner Res 2016;31(12):2085-97. DOI: 10.1002/jbmr.2913
33. Mullin BH, Zhao JH, Brown SJ, Perry J, Luan J, Zheng H-F, et al. Genome-wide association study meta-analysis for quantitative ultrasound parameters of bone identifies five novel loci for broadband ultrasound attenuation. Hum Mol Genet 2017;26(14):2791-802. DOI: 10.1093/hmg/ddx174
34. Kemp JP, Morris JA, Medina-Gomez C, Forgetta V, Warrington NM, Youlten SE, et al. Identification of 153 new loci associated with heel bone mineral density and functional involvement of GPC6 in osteoporosis. Nat Genet 2017;49(10):1468-75. DOI: 10.1038/ng.3949
35. Hollander W, Boer CG, Hart DJ, Yau MS, Ramos Y, Metrustry S, et al. Genome-wide association and functional studies identify a role for matrix Gla protein in osteoarthritis of the hand. Ann Rheum Dis 2017;76(12):2046-53. DOI: 10.1136/annrheumdis-2017-211214
36. Medina-Gomez C, Kemp JP, Trajanoska K, Luan J, Chesi A, Ahluwalia TS, et al. Life-course genome-wide association study meta-analysis of total body BMD and assessment of age-specific effects. Am J Hum Genet 2018;102(1):88-102. DOI: 10.1016/j.ajhg.2017.12.005
37. Pei Y-F, Hu W-Z, Yan M-W, Li C-W, Liu L, Yang X-L, et al. Joint study of two genome-wide association meta-analyses identified 20p12.1 and 20q13.33 for bone mineral density. Bone 2018;110:378-85. DOI: 10.1016/j.bone.2018.02.027
38. Alonso N, Estrada K, Albagha OME, Herrera L, Reppe S, Olstad OK, et al. Identification of a novel locus on chromosome 2q13, which predisposes to clinical vertebral fractures independently of bone density. Ann Rheum Dis 2018;77(3):378-85. DOI: 10.1136/annrheumdis-2017-212469
39. Kim SK. Identification of 613 new loci associated with heel bone mineral density and a polygenic risk score for bone mineral density, osteoporosis and fracture. PloS One 2018;13(7):e0200785. DOI: 10.1371/journal.pone.0200785
40. Baird DA, Evans DS, Kamanu FK, Gregory JS, Saunders FR, Giuraniuc CV, et al. Identification of novel loci associated with hip shape: a meta-analysis of genome wide association studies. J Bone Miner Res 2019;34(2):241-51. DOI: 10.1002/jbmr.3605
41. Hsu Y-H, Estrada K, Evangelou E, Ackert-Bicknell C, Akesson K, Beck T, et al. Meta-analysis of genomewide association studies reveals genetic variants for hip bone geometry. J Bone Miner Re. 2019;34(7):1284-96. DOI: 10.1002/jbmr.3698
42. Pei YF, Liu L, Liu TL, Yang XL, Zhang H, Wei XT, et al. Joint association analysis identified 18 new loci for bone mineral density. J Bone Miner Re. 2019;34(6):1086-94. DOI: 10.1002/jbmr.3681
43. Styrkarsdottir U, Stefansson OA, Gunnarsdottir K, Thorleifsson G, Lund SH, Stefansdottir L, et al. GWAS of bone size yields twelve loci that also affect height, BMD, osteoarthritis or fractures. Nat Commun 2019;10(1):2054.
44. Zheng J, Maerz W, Gergei I, Kleber M, Drechsler C, Wanner C, et al. Mendelian randomization analysis reveals a causal influence of circulating sclerostin levels on bone mineral density and fractures. J Bone Miner Res 2019;34(10):1824-36. DOI: 10.1038/s41467-019-09860-0
45. Feng GJ, Wei XT, Zhang H, Yang XL, Shen H, Tian Q, et al. Identification of pleiotropic loci underlying hip bone mineral density and trunk lean mass. J Hum Genet 2020;66(3):251-60. DOI: 10.1038/s10038-020-00835-4
46. Zhang YX, Zhang SS, Ran S, Liu Y, Zhang H, Yang XL, et al. Three pleiotropic loci associated with bone mineral density and lean body mass. Mol Genet Genomics 2020;296(1):55-65. DOI: 10.1007/s00438-020-01724-3
47. Surakka I, Fritsche LG, Zhou W, Backman J, Kosmicki JA, Lu H, et al. MEPE loss-of-function variant associates with decreased bone mineral density and increased fracture risk. Nat Commun 2020;11(1):4093. DOI: 10.1038/s41467-020-17315-0
48. Greenbaum J, Su KJ, Zhang X, Liu Y, Liu A, Zhao LJ, et al. A multiethnic whole genome sequencing study to identify novel loci for bone mineral density. Hum Mol Genet 2022;31(7):1067-81. DOI: 10.1093/hmg/ddab305
49. Leupin O, Piters E, Halleux C, Hu S, Kramer I, Morvan F, et al. Bone overgrowth-associated mutations in the LRP4 gene impair sclerostin facilitator function. J Biol Chem 2011;286(22):19489-500. DOI: 10.1074/jbc.M110.190330
50. Choi HY, Dieckmann M, Herz J, Niemeier A. Lrp4, a novel receptor for Dickkopf 1 and sclerostin, is expressed by osteoblasts and regulates bone growth and turnover in vivo. PloS One 2009;4(11):e7930. DOI: 10.1371/journal.pone.0007930
51. Chang M-K, Kramer I, Huber T, Kinzel B, Guth-Gundel S, Leupin O, et al. Disruption of Lrp4 function by genetic deletion or phar-

macological blockade increases bone mass and serum sclerostin levels. Proc Natl Acad Sci USA 2014;111(48):E5187-195. DOI: 10.1073/pnas.1413828111
52. Wang R, Zhao P, Kong N, Lu R, Pei Y, Huang C, et al. Genome-wide identification and characterization of the potato bHLH transcription factor family. Genes 2018;22;9(1):54. DOI: 10.3390/genes9010054
53. Velázquez-Cruz R, Jiménez-Ortega RF, Parra-Torres AY, Castillejos-López M, Patiño N, Quiterio M, et al. Analysis of association of MEF2C, SOST and JAG1 genes with bone mineral density in Mexican-Mestizo postmenopausal women. BMC Musculoskelet Disord 2014;15:400. DOI: 10.1186/1471-2474-15-400
54. Cosman F, Crittenden DB, Adachi JD, Binkley N, Czerwinski E, Ferrari S, et al. Romosozumab treatment in postmenopausal women with osteoporosis. N Engl J Med 2016;375(16):1532-43. DOI: 10.1056/NEJMoa1607948
55. McClung MR, Grauer A, Boonen S, Bolognese MA, Brown JP, Diez-Perez A, et al. Romosozumab in postmenopausal women with low bone mineral density. N Engl J Med 2014;370(5):412-20. DOI: 10.1056/NEJMoa1305224
56. Recker RR, Benson CT, Matsumoto T, Bolognese MA, Robins DA, Alam J, et al. A randomized, double-blind phase 2 clinical trial of blosozumab, a sclerostin antibody, in postmenopausal women with low bone mineral density. J Bone Miner Res 2015;30(2):216-24. DOI: 10.1002/jbmr.2351
57. Langdahl BL, Libanati C, Crittenden DB, Bolognese MA, Brown JP, et al. Romosozumab (sclerostin monoclonal antibody) versus teriparatide in postmenopausal women with osteoporosis transitioning from oral bisphosphonate therapy: a randomised, open-label, phase 3 trial. Lancet 2017;390(10102):1585-94. DOI: 10.1016/S0140-6736(17)31613-6
58. Glorieux FH, Devogelaer JP, Durigova M, Goemaere S, Hemsley S, Jakob F, et al. BPS804 anti-sclerostin antibody in adults with moderate osteogenesis imperfecta: results of a randomized phase 2a trial. J Bone Miner Res 2017;32(7):1496-504. DOI: 10.1002/jbmr.3143
59. Lewiecki M, Blicharski T, Goemaere S, Lippuner K, Meisner PD, Miller PD, et al. A phase III randomized placebo-controlled trial to evaluate efficacy and safety of romosozumab in men with osteoporosis. J Clin Endocrinol Metab 2018;103(9):3183-93. DOI: 10.1210/jc.2017-02163
60. Martínez-Gil N, Ugartondo N, Grinberg D, Balcells S. Wnt pathway extracellular components and their essential roles in bone homeostasis. Genes (Basel) 2022;13(1):138. DOI: 10.3390/genes13010138
61. Balemans W, Patel N, Ebeling M, Van Hul E, Wuyts W, Lacza C, et al. Identification of a 52 kb deletion downstream of the SOST gene in patients with van Buchem disease. J Med Genet 2002;39(2):91-7. DOI: 10.1136/jmg.39.2.91
62. Sebastian A, Loots GG. Genetics of Sost/SOST in sclerosteosis and van Buchem disease animal models. Metabolism 2018;80:38-47. DOI: 10.1016/j.metabol.2017.10.005
63. Collette NM, Genetos DC, Economides AN, Xie L, Shahnazari M, Yao W, et al. Targeted deletion of Sost distal enhancer increases bone formation and bone mass. Proc Natl Acad Sci USA 2012;109(35):14092-7. DOI: 10.1073/pnas.1207188109
64. Martínez-Gil N, Roca-Ayats N, Cozar M, Garcia-Giralt N, Ovejero D, Nogués X, et al. Genetics and genomics of SOST: functional analysis of variants and genomic regulation in osteoblasts. Int J Mol Sci 2021;22(2):489. DOI: 10.3390/ijms22020489
65. Loots G, Kneissel M, Keller H, Baptist M, Chang J, Collette NM, et al. Genomic deletion of a long-range bone enhancer misregulates sclerostin in Van Buchem disease. Genome Res 2005;15(7):928-35. DOI: 10.1101/gr.3437105
66. Kramer I, Baertschi S, Halleux C, Keller H, Kneissel M. Mef2c deletion in osteocytes results in increased bone mass. J Bone Miner Res 2012;27(2):360-73. DOI: 10.1002/jbmr.1492
67. Duncan E, Danoy P, Kemp JP, Leo PJ, McCloskey E, Nicholson GC, et al. Genome-wide association study using extreme truncate selection identifies novel genes affecting bone mineral density and fracture risk. PLoS Genet 2011;7(4):e1001372. Genome-wide association study using extreme truncate selection identifies novel genes affecting bone mineral density and fracture risk
68. Pei YF, Hu WZ, Hai R, Wang XY, Ran S, Lin Y, et al. Genome-wide association meta-analyses identified 1q43 and 2q32.2 for hip Ward's triangle areal bone mineral density. Bone 2016;91:1-10. DOI: 10.1016/j.bone.2016.07.004
69. Zheng HF, Duncan EL, Yerges-Armstrong LM, Eriksson J, Bergström U, Leo PJ, et al. Meta-analysis of genome-wide studies identifies MEF2C SNPs associated with bone mineral density at forearm. J Med Genet 2013;50(7):473-8. DOI: 10.1136/jmedgenet-2012-101287
70. Gregson CL, Newell F, Leo PJ, Clark GR, Paternoster L, Marshall M, et al. Genome-wide association study of extreme high bone mass: contribution of common genetic variation to extreme BMD phenotypes and potential novel BMD-associated genes. Bone 2018;114:62-71. DOI: 10.1016/j.bone.2018.06.001
71. Baertschi S, Baur N, Lueders-Lefevre V, Voshol J, Keller H. Class I and IIa histone deacetylases have opposite effects on sclerostin gene regulation. J Biol Chem 2014;289(36):24995-5009. DOI: 10.1074/jbc.M114.564997
72. Kobayashi Y, Uehara S, Koide M. Regulations of osteoclast formation and function by Wnt signals. Clin Calcium 2019;29(3):309-15. DOI: 10.20837/4201903309
73. Wein M, Fretwurst T, Nahles S, Duttenhoefer F, Tomakidi P, Steinberg T, et al. Pilot investigation of the molecular discrimination of human osteoblasts from different bone entities. J Craniomaxillofac Surg 2015;43(8):1487-93. DOI: 10.1016/j.jcms.2015.07.030
74. Kichaev G, Bhatia G, Loh PR, Gazal S, Burch K, Freund MK, et al. Leveraging polygenic functional enrichment to improve GWAS power. Am J Hum Genet 2019;104(1):65-75.
75. Kawano Y, Kypta R. Secreted antagonists of the Wnt signalling pathway. J Cell Sci 2003;116(13):2627-34. DOI: 10.1016/j.jcms.2015.07.030
76. Glinka A, Wu W, Delius H, Monaghan AP, Blumenstock C, Niehrs C. Dickkopf-1 is a member of a new family of secreted proteins and functions in head induction. Nature 1998;391(6665):357-62. DOI: 10.1038/34848
77. Ai M, Heeger S, Bartels CF, Schelling DK, Osteoporosis-Pseudoglioma Collaborative Group. Clinical and molecular findings in osteoporosis-pseudoglioma syndrome. Am J Hum Genet 2005;77(5):741-53. DOI: 10.1086/497706
78. Balemans W, Devogelaer JP, Cleiren E, Piters E, Caussin E, Van Hul W. Novel LRP5 missense mutation in a patient with a high bone mass phenotype results in decreased DKK1-mediated inhibition of Wnt signaling. J Bone Miner Res 2007;22(5):708-16. DOI: 10.1359/jbmr.070211

79. Martínez-Gil N, Roca-Ayats N, Monistrol-Mula A, García-Giralt N, Díez-Pérez A, Nogués X, et al. Common and rare variants of WNT16, DKK1 and SOST and their relationship with bone mineral density. Sci Rep 2018;8(1):10951. DOI: 10.1038/s41598-018-29242-8
80. Korvala J, Löija M, Mäkitie O, Sochett E, Jüppner H, Schnabel D, et al. Rare variations in WNT3A and DKK1 may predispose carriers to primary osteoporosis. Eur J Med Genet 2012;55(10):515-9. DOI: 10.1016/j.ejmg.2012.06.011
81. van de Putte R, Wijers CH, de Blaauw I, Feitz WF, Marcelis CL, Hakobjan M, et al. Sequencing of the DKK1 gene in patients with anorectal malformations and hypospadias. Eur J Pediatr 2015;174(5):583-7. DOI: 10.1007/s00431-014-2436-x
82. Ntini E, Louloupi A, Liz J, Muino JM, Marsico A, Vang-Ørom UA. Long ncRNA A-ROD activates its target gene DKK1 at its release from chromatin. Nat Commun 2018;9(1):1636. DOI: 10.1038/s41467-018-04100-3
83. Zheng H-F, Tobias JH, Duncan E, Evans DM, Eriksson J, Paternoster L, et al. WNT16 influences bone mineral density, cortical bone thickness, bone strength, and osteoporotic fracture risk. PLoS Genet 2012;8(7):e1002745. DOI: 10.1371/journal.pgen.1002745
84. Movérare-Skrtic S, Henning P, Liu X, Nagano K, Saito H, Börjesson AE, et al. Osteoblast-derived WNT16 represses osteoclastogenesis and prevents cortical bone fragility fractures. Nat Med 2014;20(11):1279-88. DOI: 10.1038/nm.3654
85. Nabbi A, Almami A, Thakur S, Suzuki K, Boland D, Bismar TA, et al. ING3 protein expression profiling in normal human tissues suggest its role in cellular growth and self-renewal. Eur J Cell Biol 2015;94(5):214-22. DOI: 10.1016/j.ejcb.2015.03.002
86. Chesi A, Wagley Y, Johnson ME, Manduchi E, Su Ch, Lu S, et al. Genome-scale capture C promoter interactions implicate effector genes at GWAS loci for bone mineral density. Nat Commun 2019;10(1):1260. DOI: 10.1038/s41467-019-09302-x
87. Maynard RD, Godfrey DA, Medina-Gomez C, Ackert-Bicknell CL. Characterization of expression and alternative splicing of the gene cadherin-like and PC esterase domain containing 1 (Cped1). Gene 2018;674:127-33. DOI: 10.1016/j.gene.2018.06.060
88. Määttä JA, Bendre A, Laanti M, Büki KG,Rantakari P, Tervola P, et al. Fam3c modulates osteogenic cell differentiation and affects bone volume and cortical bone mineral density. Bonekey Rep 2016;5:787. DOI: 10.1038/bonekey.2016.14
89. Bendre A, Büki KG, Määttä JA. Fam3c modulates osteogenic differentiation by down-regulating Runx2. Differentiation 2017;93:50-7. DOI: 10.1016/j.diff.2016.11.005
90. Martínez-Gil N, Patiño J, Ugartondo N, Grinberg D, Balcells S. WNT16 rs2908004 missense variant acts as eQTL of FAM3C in human primary osteoblasts. Rev Osteoporos Metab Miner 2021;13(4):117-21.
91. Martínez-Gil N, Roca-Ayats N, Herrera C, Gritti N, Ugartondo N, Garcia-Giralt N, et al. Functional evidence of bone regulation of WNT16 through upstream enhancers within CPED1. J Bone Miner Res 2020;35S1:179.

Revista de Osteoporosis y Metabolismo Mineral

Image in Osteology

Saber tibia

Jesús Rubio Úbeda, Inmaculada Jiménez Moleón, Enrique Raya Álvarez

Rheumatology Service. Hospital Universitario Clínico San Cecilio. Granada, Spain

CASE REPORT

A 91-year-old woman presented with a 6-month history of pain in the right tibial region, associated with bone deformity and progressive difficulty in walking. Physical examination confirmed these findings, also highlighting an increase in local temperature in the right tibial region.

A basic analytical study with biochemistry and complete blood count was carried out, including phosphocalcic metabolism parameters and bone remodeling markers. Raised levels of alkaline phosphatase (AP) in serum (141 U/L [N = 30-120]) were observed, as well as elevation of bone formation markers (type I collagen amino-terminal propeptide [PINP] 166 ng/mL, [N = 20.2-76.3]) and bone resorption markers (β-Cross-Laps [β-CTX] 0.042 ng/mL [N = 0.000-0.028] and C-terminal telopeptide [ICTP] 1.28 ng/mL [N = 0.556-1]).

Imaging included X-rays of long bones, pelvis, thoracolumbar spine and skull which revealed a characteristic image of saber shin at the level of the right tibia (Figs. 1-3), and bone scan with ^{99m}Tc-HDA (Fig. 4). Given these test results, and after only finding alterations (both structural and metabolic) at the level of the right tibia, the patient was finally diagnosed with monostotic Paget's disease of bone.

DISCUSSION

The case presented is paradigmatic of Paget's bone disease with a saber tibial deformity. In our case, late diagnosis takes on a special meaning insofar as the observed deformity must have developed over decades without having been diagnosed until then. These highlights the importance of detecting deformities of the musculoskeletal system in any basic examination carried out in a consultation to avoid both its progression and complications derived from the disease itself.

Received: 24/06/202 • Accepted: 10/10/2022

Conflict of interests: the authors declare no conflict of interest.

Rubio Úbeda J, Jiménez Moleón I, Raya Álvarez E. Saber tibia. Rev Osteoporos Metab Miner 2023;15(1):40-42

DOI: 10.20960/RevOsteoporosMetabMiner.00009

CLINICAL IMAGES

Figure 1. X-ray of the right femur and femorotibial joint: the contrast between the fine reticular trabecular pattern of the femur and the coarse and aberrant trabeculation observed in the tibial plateau stands out. Femorotibial and patellofemoral osteoarthritis. As an incidental finding, calcification of the femoropopliteal artery.

Figures 2 and 3. Radiographs of the right tibia. Saber tibia: increased cortical and periosteal thickness, with a coarse and disordered trabecular pattern, as well as a large tibial deformity, which curves laterally with a saber appearance.

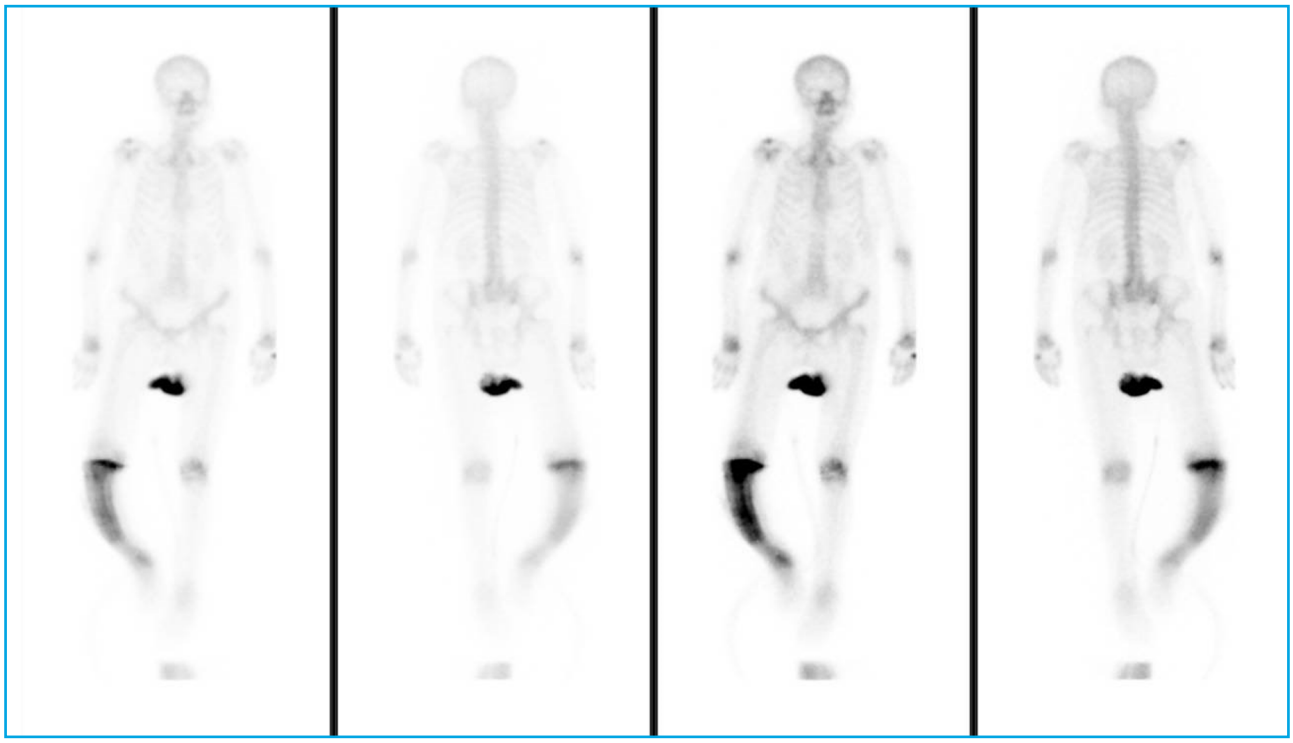

Figure 4. Whole-body bone scan with ^{99m}Tc-HAD. Uptake of moderate/severe intensity is observed in the right tibia. In the rest of the skeleton, a more diffuse and less intense deposit can be seen in the shoulders, elbows, wrists and left knee with degenerative characteristics.